Early to middle Eocene magneto-biochronology of the southwest Pacific Ocean and climate influence on sedimentation: Insights from the Mead Stream section, New Zealand

Edoardo Dallanave[1,†], Claudia Agnini[2], Valerian Bachtadse[1], Giovanni Muttoni[3,4], James S. Crampton[5,6], C. Percy Strong[5], Benjamin R. Hines[6], Christopher J. Hollis[5], and Benjamin S. Slotnick[7]

[1]*Department of Earth and Environmental Science, Ludwig-Maximilians University, Theresienstrasse 41, Munich D-80333, Germany*
[2]*Department of Geosciences, University of Padova, Via G. Gradenigo 6, I-35131 Padova, Italy*
[3]*Department of Earth Sciences, University of Milan, Via Mangiagalli 34, I-20133 Milano, Italy*
[4]*Alpine Laboratory of Paleomagnetism (ALP), Via Luigi Massa 6, I-12016 Peveragno (CN), Italy*
[5]*GNS Science, P.O. Box 30368, Lower Hutt 5040, New Zealand*
[6]*School of Geography, Environment and Earth Sciences, Victoria University of Wellington, Private Bag 600, Wellington, New Zealand*
[7]*Department of Earth Sciences, Rice University, Houston, Texas 77005, USA*

ABSTRACT

The Mead Stream section (South Island, New Zealand) consists of a 650-m-thick series of continuous, well-exposed strata deposited on a South Pacific continental slope from the Late Cretaceous to the middle Eocene. We examined the uppermost Paleocene–middle Eocene part of the section, which consists of ~360 m of limestone and marl, for detailed magnetic polarity stratigraphy and calcareous nannofossil and foraminifera biostratigraphy. Magneto-biostratigraphic data indicate that the section straddles magnetic polarity chrons from C24r to C18n, calcareous nannofossil zones from NP9a to NP17 (CNP11–CNE15, following a recently revised Paleogene zonation), and from the Waipawan to the Bortonian New Zealand stages (i.e., from the base of the Ypresian to the Bartonian international stages). The Mead Stream section thus encompasses 17 m.y. (56–39 Ma) of southwest Pacific Ocean history. The ages of calcareous nannofossil biohorizons are consistent with low- to midlatitude data from the literature, indicating that during the early–middle Eocene, the low- to midlatitude calcareous nannofossil domain extended at least to ~50°S–55°S in the South Pacific. Correlation of the magnetic polarity stratigraphy from the Mead Stream section with the geomagnetic polarity time scale allows us to derive sediment accumulation rates (SAR), which range between 8 and 44 m/m.y. Comparing the SAR with paleotemperature proxy records, we found that two intervals of increased SAR occurred during the early Eocene climatic optimum (52–50 Ma) and during the transient warming event peaking with the middle Eocene climatic optimum (40.5 Ma). This correlation indicates that, at Mead Stream, the climate evolution of the early–middle Eocene is recorded in a sedimentation pattern whereby, on a million-year time scale, warmer climate promoted continental weathering, transportation, and accumulation of terrigenous sediments.

INTRODUCTION

The Eocene Epoch records progressive global cooling from the warm climates of the early Eocene climatic optimum (ca. 52–50 Ma) to the first major inception of Antarctic ice sheets at the Eocene-Oligocene boundary (ca. 34 Ma; Zachos et al., 2001, 2008). To understand the nature and causes of this global climate evolution, it is critical to construct robust chronologies of continental and marine sedimentary records deposited at different paleolatitudes in both hemispheres. The Northern Hemisphere is now relatively well represented with magnetostratigraphically calibrated Tethyan marine records that crop out in the southern Alps and Apennines of Italy, such as Possagno (Agnini et al., 2006), Cicogna (Dallanave et al., 2009), Alano (Agnini et al., 2011), and Contessa Highway (Lowrie and Alvarez, 1977; Jovane et al., 2007). Significant deep-sea sedimentary records from the Northern Hemisphere include Ocean Drilling Program (ODP) Site 1220 (Leg 199, tropical Pacific; Lyle et al., 2002; Parès and Lanci, 2004), and Site 1051A (Leg 171b, Blake Nose; Edgar et al., 2010; Ogg and Bardot, 2001) (Fig. 1).

For the Southern Hemisphere, Eocene magnetostratigraphy and calcareous nannofossil and planktic foraminifera biostratigraphy data have been obtained from ODP Site 690 (Leg 113, Maud Rise; Florindo and Roberts, 2005; Thomas et al., 1990), ODP Site 702 (Leg 114, Isla Orcadas Rise; Clement and Hailwood, 1991; Fioroni et al., 2012), and ODP Site 762 (Leg 122, Exmouth Plateau, northwest Australian margin; Hancock et al., 2002; Galbrun, 1992). These records, however, contain several core gaps and are not continuous. In the last few years, information on the marine temperature of the southern Pacific and Southern Ocean throughout the Eocene has been obtained from paleoclimate proxy records from the Canterbury Basin, New Zealand (Burgess et al., 2008; Hollis et al., 2009, 2012; Pancost et al., 2013), from ODP Site 1172, Leg 189, East Tasman Plateau (Bijl et al., 2009, 2013), and from Integrated Ocean Drilling Program (IODP) Site U1356, Expedition 318, Wilkes Land Margin, Antarctica (Pross et al., 2012). The chronology of these records is, however, poorly constrained, because a good magnetostratigraphic record is still missing (see Tauxe et al., 2012).

In this paper, we present results from the marine succession outcropping along Mead Stream in the Clarence Valley, eastern Marlborough, New Zealand (Strong et al., 1995). Sediments were originally deposited on a

†dallanave@geophysik.uni-muenchen.de

GSA Bulletin; doi: 10.1130/B31147.1; 9 figures; 2 tables.

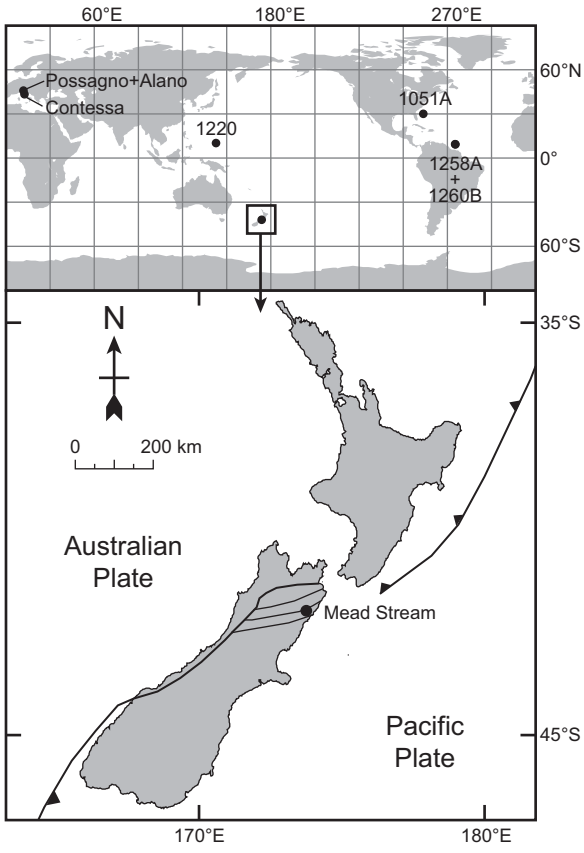

Figure 1. Location of the Mead Stream section (173.79°E, 41.96°S) and of the early Paleogene reference sections and deep-sea sites discussed in the text and shown in Figure 7.

carbonate ramp on a northwest-facing reentrant of the New Zealand northern paleo–margin (Crampton et al., 2003). The Mead Stream section, which includes Late Cretaceous to middle Eocene sequences (Strong et al., 1995), contains the most complete, continuous, and expanded early Paleogene stratigraphic record of the South Pacific. It has been the subject of numerous studies, which have focused on the sedimentary and paleoecological response to climatic change through the late Paleocene–early Eocene (Hancock et al., 2003; Hollis et al., 2005a, 2005b; Nicolo et al., 2007, 2010; Slotnick et al., 2012). In particular, the isotope record derived from these previous studies provides important information about an evolving late Paleocene–early Eocene carbon cycle (Nicolo et al., 2007, 2010; Slotnick et al., 2012). Rock-magnetic properties of exposed sediments have been also investigated across the Paleocene-Eocene boundary (Villasante-Marcos et al., 2009). A general increase of initial magnetic susceptibility and saturation isothermal remanent magnetization (IRM) across the Paleocene–Eocene thermal maximum (e.g., Kennett and Stott, 1991), integrated with lithology and carbon isotope data (Hancock et al., 2003; Hollis et al., 2005a; Nicolo et al., 2007, 2010), indicates that the Paleocene–Eocene thermal maximum record is characterized by increased terrigenous input, related to an enhanced hydrological cycle and increased terrestrial discharge during a time of global warming (Nicolo et al., 2007; Slotnick et al., 2012). However, the age-calibration of this stratigraphic record has been thus far hampered by the apparent absence of age-diagnostic low-latitude bioevents and difficulties in recovering a paleomagnetic signature that yields a coherent magnetostratigraphy (Hollis et al., 2005a; Kodama et al., 2007; Nicolo et al., 2007; Slotnick et al., 2012).

Here, we report the first successful recovery of a coherent magnetostratigraphy for the early to middle Eocene at Mead Stream (Fig. 1), the most-studied and probably most complete of the Clarence Valley sections. Our magnetostratigraphy is complemented by a new quantitative study of calcareous nannofossils and a review of planktic foraminiferal biostratigraphy. The results are compared to published coeval records from low- to midlatitude settings. We also examine the relationship between sediment accumulation rates (SAR) of the Mead Stream section, derived by correlation with the Ogg and Smith (2012) geomagnetic polarity time scale (GPTS12), and the Eocene paleotemperature evolution as revealed by published marine paleotemperature proxies.

GEOLOGIC AND STRATIGRAPHIC FRAMEWORK

Lithostratigraphy

Muzzle Group

During the Late Cretaceous–early Paleogene, several sedimentary basins formed and deepened in the New Zealand region as a consequence of passive-margin thermal subsidence (Ballance, 1993; King et al., 1999). In eastern Marlborough, the Late Cretaceous–middle Eocene sediments of the Muzzle Group were deposited in shelfal to bathyal environments, from the outer shelf to the upper slope at the southern margin of the East Coast Basin (summarized in Crampton et al., 2003). Neogene deformation uplifted and folded the succession (Field et al., 1997; Crampton et al., 2003), so that now the NW-dipping Muzzle Group sediments crop out in the beds and banks of a series of SW-flowing tributaries of the Clarence River. Several works can provide an overview about the geology and stratigraphy of the area (e.g., Reay, 1993; Strong et al., 1995; Hollis et al., 2005a, 2005b).

Mead Stream Section

The Mead Stream section contains the thickest and most complete record of the Muzzle Group (Strong et al., 1995; Hollis et al., 2005a), consisting of ~650 m of strata with excellent exposure (>90%). The Upper Paleocene to Middle Eocene Amuri Limestone of the Muzzle Group is subdivided into four lithotypes (Reay, 1993; Strong et al., 1995), which are, from bottom to top: (1) Lower Limestone, (2) Lower Marl, (3) Upper Limestone, and (4) Upper Marl (Fig. 2). The base of the section sampled for calcareous nannofossils is placed at meter level 150 above the level containing the Cretaceous-Paleogene boundary (meter level 0), while the paleomagnetic sampling began at 180 m. The Lower Limestone consists of decimeter-thick limestone beds with marl horizons or partings. The contact between the Lower Limestone and Lower Marl is gradational and is placed 204 m above the Cretaceous-Paleogene boundary, where thick marl beds become numerous (Hollis et al., 2005a). The Lower Marl is 116 m-thick and consists of alternating gray-green soft marls and well-indurated limestones. Between 270 m and 315 m, local folding and faulting interrupt the regular stratification of the Lower Marl unit. The overlying Upper Limestone, the base of which is placed at 320 m, is 76 m-thick and consists of decimeter-thick, white and highly indurated limestone beds with stylolitic partings. The base of the uppermost unit, the Upper Marl, is placed at 397 m. This unit consists of 119 m of gray-green soft marls interbedded

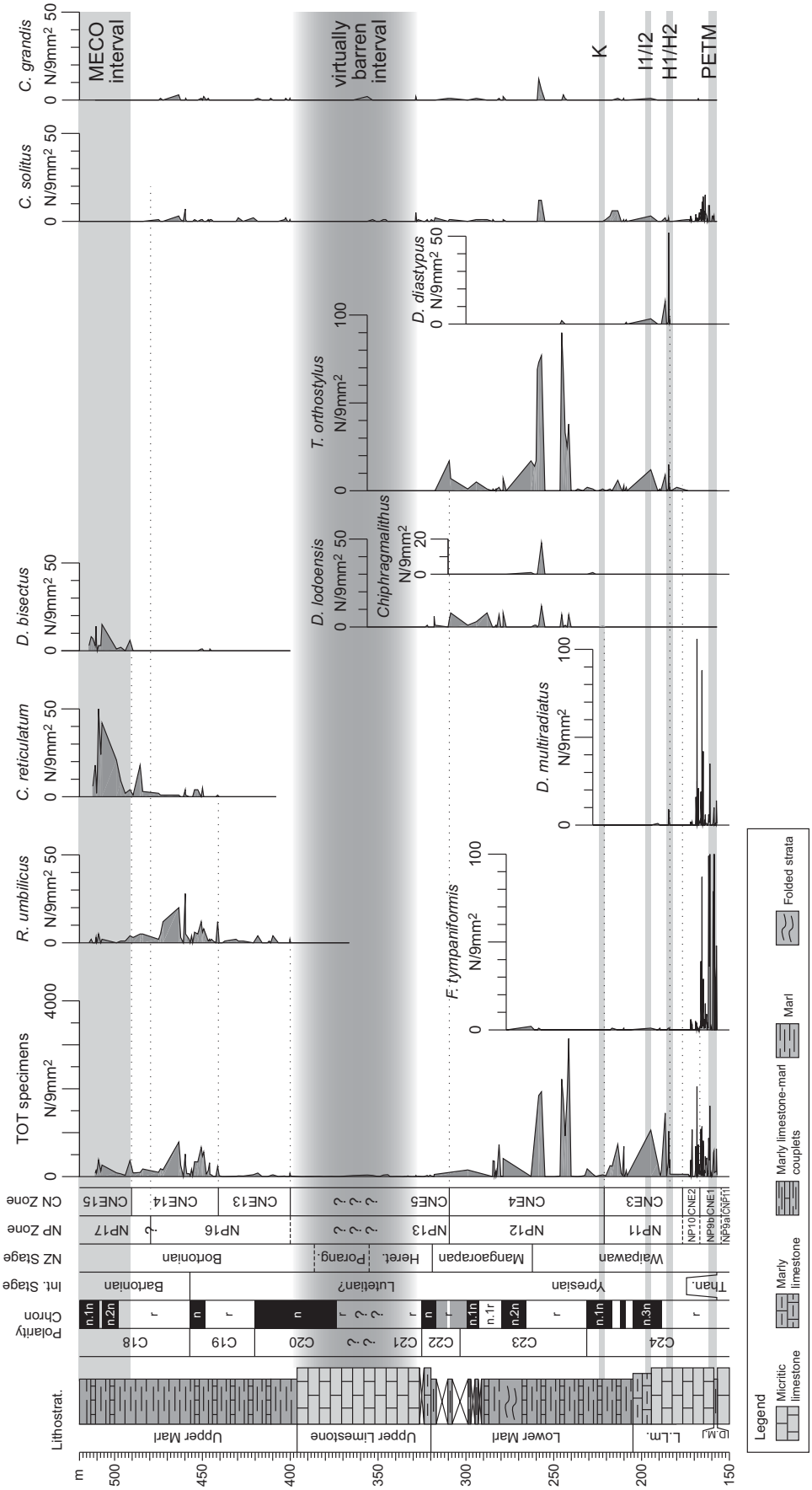

Figure 2. Litho- and biostratigraphy of the Mead Stream section. From left to right: Lithostratigraphy plotted against stratigraphic position (L. Lm.—Lower Limestone; D.M.—Dee marl); magnetic polarity stratigraphy (summarized from Fig. 4); international stage New Zealand stage boundary positions as determined by foraminiferal biostratigraphy; calcareous nannofossil biostratigraphy: NP zones (Martini, 1971) and CN zones (Agnini et al., 2014); total abundance of calcareous nannofossils and abundance patterns of selected calcareous nannofossil taxa. The positions of the hyperthermal events (Paleocene Eocene thermal maximum [PETM], H1/H2, I1/I2, K events as defined by Cramer et al. [2003], and the middle Eocene climatic optimum [MECO]) are from Slotnick et al. (2012).

with moderately indurated limestones. The top of the Upper Marl is unconformably overlain by the late Oligocene–early Miocene Weka Pass Stone Formation (Strong et al., 1995), starting at 523 m (not sampled).

Biostratigraphy and Carbon Isotope Stratigraphy

The first biostratigraphic framework for the Amuri Limestone at Mead Stream was presented by Strong et al. (1995). These data include foraminiferal, radiolarian, and dinoflagellate biostratigraphy, and they indicate that the Amuri Limestone spans from the late Teurian to the Bortonian New Zealand stages, corresponding to late Paleocene to middle Eocene. The litho-biostratigraphic data set of the Paleocene–early Eocene part of the Amuri Limestone (i.e., up to lowermost Lower Marl) was refined by Hollis et al. (2005a), who provided a detailed lithologic description integrated with bulk carbonate carbon isotopes, radiolarian, calcareous nannofossil, and foraminiferal biostratigraphy. The carbon isotope record across the Lower Limestone and Lower Marl presented by Hollis et al. (2005a) has been updated and refined by Nicolo et al. (2007) and later by Slotnick et al. (2012), who correlated the sequence of negative carbon isotope excursions with early Eocene hyperthermals from the Paleocene–Eocene thermal maximum (Kennett and Stott, 1991; McInerney and Wing, 2011) to ~21 m above the early Eocene "L" event of Cramer et al. (2003). This data set has been used to derive a first age model for the Mead Stream section (Slotnick et al., 2012) by means of correlation with coeval magnetostratigraphically calibrated carbon isotope records from ODP Site 1262 (Leg 208, southeastern Atlantic Ocean; Agnini et al., 2007; Zachos et al., 2010) and Deep Sea Drilling Project (DSDP) Site 577 (Leg 86, North Pacific Ocean; Shackleton et al., 1985; Cramer et al., 2003; Dickens and Backman, 2013).

MATERIAL AND METHODS

Rock- and Paleomagnetism

Paleomagnetic samples were drilled in the field with a gasoline-powered drill and were oriented with a magnetic compass during the March 2012 expedition conducted after a preliminary survey in 2010. In total, 248 oriented cores were collected across 340 m of the Mead Stream section (from 180 to 520 m) at an average sampling resolution of one core per ~1.4 m. From these cores, we obtained 293 standard ~11 cm^3 specimens for paleomagnetic analysis. We used a representative set of specimens from the trimmed ends of the cores to investigate the magnetic properties of the sediments by means of stepwise IRM acquisition curves. The curves were examined using cumulative log Gaussian analysis following Kruiver et al. (2001). The coercivity of remanence (B_{cr}) of the specimens was then determined by applying a stepwise backfield IRM (BIRM) up to a maximum of 60 mT. The same specimens were then exposed to three orthogonal IRMs imparted at fields of 2.5 T, 0.4 T, and 0.12 T, which were thermally demagnetized in 16 consecutive steps from room temperature up to 600 °C (Lowrie, 1990). Sister specimens were subjected to thermomagnetic analyses. They were heated in air up to 650 °C in an inducing field of 800 mT using a variable-field translation balance (VFTB; Krása et al., 2007). The Curie temperatures of the heating cycles were determined by analysis of the second derivative curves (Tauxe, 2010).

The natural remanent magnetization (NRM) of the oriented samples was initially studied by means of alternating field (AF) or thermal demagnetization. A first set of 68 specimens was subjected to three-axis AF static demagnetization in 12 increasing peak fields from 3 mT to 90 mT. Some of the AF-treated specimens acquired a gyro-remanent magnetization (GRM) at fields ≥50 mT. For this reason, the remaining 225 specimens were all thermally demagnetized with steps of 50 °C (reduced to 25 °C from 450 °C onward) up to a maximum temperature of 575 °C. The NRM of the specimens was measured after each demagnetization step using a 2-G Enterprises DC SQUID cryogenic magnetometer placed in a shielded room. NRM components were examined by applying the standard least-square analysis of Kirschvink (1980) on linear segments of vector end-point demagnetization diagrams (Zijderveld, 1967). Mean directions and associated statistical parameters were calculated using the spherical statistics of Fisher (1953). Directional analyses were performed with the PaleoMag software of Jones (2002). All analyses were conducted at the paleomagnetic laboratory of Ludwig-Maximilian University (Munich, Germany) and at the Alpine Laboratory of Paleomagnetism (ALP; Cuneo, Italy).

Calcareous Nannofossils

The calcareous nannofossil data set presented here is based on a suite of 260 samples collected from several expeditions to Mead Stream from 1991 to 2012. The investigated part of the section extends from 157.07 m to 514.60 m, immediately above the initial abrupt drop in $\delta^{13}C$ at ~156.80 m, referred to as the "c" event (Bains, 1999), which is used to define the base of the Ypresian (base of Eocene and of the Waipawan local stage). Biohorizons below this level, used to define the base of subzone NP9b and zone CNE1, are after Hollis et al. (2005a). Smear slides, prepared using standard techniques as described in Bown and Young (1998), were scrutinized under a Zeiss light microscope at 1250× magnification. To identify calcareous nannofossils, we followed the taxonomic concepts of Aubry (1984, 1988, 1989, 1990, 1999), Perch-Nielsen (1985), and Bown (2005). For biostratigraphic classification of the section, we used three types of biohorizons: base (B), base common and continuous (Bc), and top (T) (Backman et al., 2012; Agnini et al., 2014). The position of the biohorizons was calculated as the midpoint between consecutive samples. The classic nannofossil biozonation schemes of Martini (1971) and Okada and Bukry (1980) are difficult to apply at Mead Stream because some of the marker species used to define zonal boundaries are not present throughout the section. The new zonal scheme proposed by Agnini et al. (2014) was instead adopted as the principal biostratigraphic framework in this study. According to a qualitative screening of the studied samples, the state of preservation of calcareous nannofossils is moderate to poor, and the abundance is highly variable, from absent to common. The numbers of specimens of selected taxa, as well as the total number of calcareous nannofossils in a prefixed area of 9 mm^2 (three traverses), were counted (following Backman and Shackleton, 1983, modified) in order to produce abundance patterns of marker species and semiquantitative estimates of calcareous nannofossil abundance, respectively.

Foraminifera

The foraminiferal data presented here are based on 26 samples collected in 2005, which extend from the lower part of the Lower Marl to the base of the Upper Marl (257.9–399 m). Samples were washed in water and sieved at 75 µm. Identifications were based on Hornibrook et al. (1989) and Pearson et al. (2006). Assignment to New Zealand stages is based on Cooper (2004) and Hollis et al. (2010), recalibrated to GPTS12.

RESULTS

Rock Magnetism

IRM acquisition curves (Fig. 3, column A) are dominated by a low-coercivity component possessing a $B_{1/2}$ (the field at which half of the saturation magnetization is reached) that ranges between 45.4 and 55.6 mT, with an average value of 49.4 mT. The B_{cr} obtained from the BIRM curves ranges between 41 and 52 mT, with an average value of 44 mT (Fig. 3, column B). The

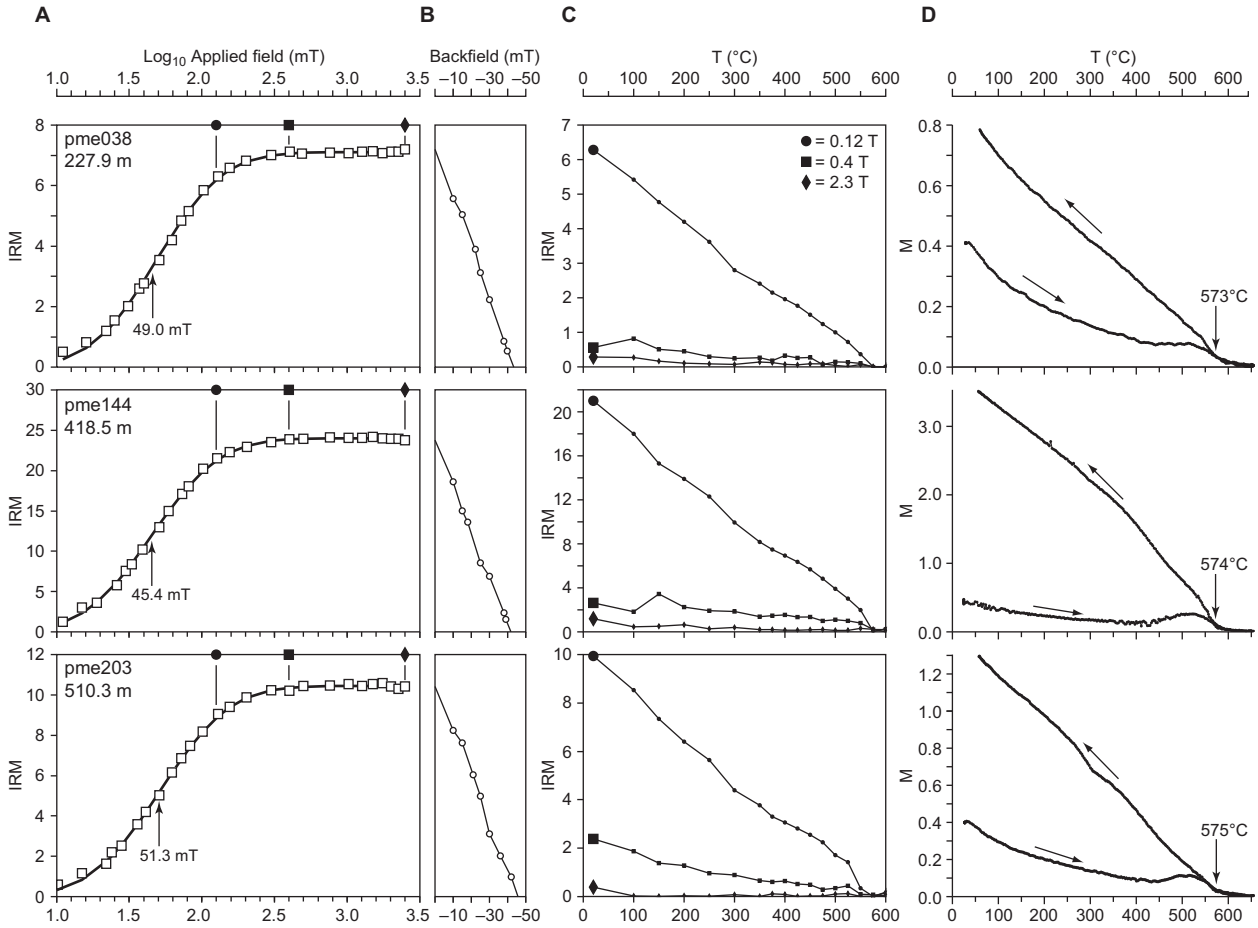

Figure 3. Rock-magnetic analyses of representative specimens from the Mead Stream section. (A) Isothermal remanent magnetization (IRM, expressed in 10^{-3} Am^{-1} in all graphs) acquisition curves; open squares represent the IRM data; the thick black line is the magnetic coercivity component; the black circles, squares, and diamonds represent the field values of 0.12 T, 0.4 T, and 2.3 T, respectively, which are the fields used for thermal demagnetization of three orthogonal IRMs shown in C. (B) IRM backfield demagnetization curves, shown to a minimum value of IRM = 0; the crossing point of the curves with the IRM = 0 axis is the coercivity of remanence (B_{cr}). (C) Thermal demagnetization of three orthogonal IRMs (Lowrie, 1990). (D) Thermomagnetic curves; M—magnetization (expressed in 10^{-1} A m^2 kg^{-1}); the temperature indicated in each graph is the Curie temperature as determined by analyses of the second derivative of the heating cycle (analysis not shown).

three component-IRM thermal demagnetization experiments (Fig. 3, column C) indicate a dominant low-coercivity (0.12 T) magnetic phase with maximum unblocking temperature of 575 °C. The heating cycles of the thermomagnetic curves (Fig. 3, column D) show a gradual decay of the magnetization, interrupted by a variable "hump" centered at around 500 °C, followed by a complete decay to zero remanence at ~575 °C. The curves are not reversible, and the cooling cycles show a gradual increase of magnetization that, at room temperature, is up to seven times greater than before heating. Similar curves have been observed in natural sediments containing ferriferous phases like pyrite (Passier et al., 2001) and siderite (Hirt and Gehring, 1991). In particular, Hirt et al. (1993) described the formation of magnetite during heating of Fe-enriched smectites, which is the dominant clay mineral in the Amuri Limestone (Fergusson, 1985; Morris, 1987). Overall, these results indicate the presence of magnetite as carrier of magnetization, with the presence of paramagnetic clay mineral (smectite) turning to magnetite during heating up to >450 °C. Despite the clay mineral content of the Mead Stream sediments due to their proximal paleogeographic position, the magnetic properties are generally consistent with those of pelagic carbonates. In the recent years, single-domain (SD) magnetite of biogenic origin has been found to be a widespread contributor to the magnetization of marine carbonates (for an overview, see Roberts et al., 2013a). The maximum unblocking temperature of 575 °C measured in the thermal demagnetization of IRM, which is also the maximum decay temperature measured in the thermomagnetic experiments, is approximately the Curie temperature of magnetite (e.g., Tauxe, 2010). The measured B_{cr} value of 44 mT is in agreement with the 40–45.5 mT value of bacterial magnetite from uncultured specimens (Pan et al., 2005). Also, the occasional occurrence of a GRM at fields ≥50 mT during AF demagnetization supports the presence of SD magnetic particles (Stephenson, 1980; Potter and Stephenson, 1986; Roberts et al., 2011). The very smooth inflection observed at ~300–400 °C in the 0.12 T branch of the IRM thermal demagnetization curves could be due to thermally induced irreversible inversion of maghemite (likely as surface coating of magnetite grains) to hematite (Deng et al., 2001; Liu et al., 2005; Dallanave et al., 2010).

Paleomagnetism

The NRM intensity is generally low, ranging from 1.6×10^{-7} to 1.7×10^{-4} Am^{-1}, with an average value of 3.8×10^{-5} Am^{-1}. The highest values are recorded in the Lower Limestone and Lower Marl (Fig. 4). The NRM drops to a minimum across the Upper Limestone, where only a few reliable characteristic remanent magnetization (ChRM) directions were isolated. Up section, NRM values increase again slightly, but they are lower than in the Lower Marl.

Scattered magnetic "A" component directions statistically oriented north-and-up were isolated up to 200–250 °C during thermal demagnetization, and at up to 12–15 mT during AF demagnetization (Fig. 5). This component falls close to the geocentric axial dipole field at the sampling location (e.g., Tauxe, 2010; Fig. 6A), and it is thus interpreted as a recent viscous magnetic overprint.

In 54% of the specimens (158/293), a ChRM trending linearly to the origin of the orthogonal projection axes has been isolated (Fig. 5). In particular, this ChRM was isolated in 35 of the 68 AF-demagnetized specimens, and in 123 of the 225 thermally demagnetized specimens. In order to visualize how the number of successfully isolated ChRM directions (*N*) varies along the section relative to the total number of demagnetized specimens (*S*), we calculated the *N*/*S* ratio using a 10 m stratigraphic window (Fig. 4). Specimens collected from the Lower Limestone and Lower Marl have generally well-defined ChRM directions, isolated up to 50–70 mT or 500–575 °C (Fig. 5A). In the lower part of the Upper Limestone, from ~331 to 370 m, where the lower NRM values are observed, the demagnetization diagrams have random behaviors (Fig. 5B, pme113a), and no ChRM directions were isolated. From 370 m through the Upper Limestone, ChRM directions were again isolated up to 400–500 °C (Fig. 5B, pme129). Several specimens (~60%) collected in the Upper Marl also have randomly oriented vector end-point diagrams, precluding isolation of ChRM directions (Fig. 5C, pme158b). In the remaining specimens from the Upper Marl, ChRM directions have been isolated up to unblocking temperatures ranging from 400 °C to 525 °C, or up to an AF field of 50 mT. Many

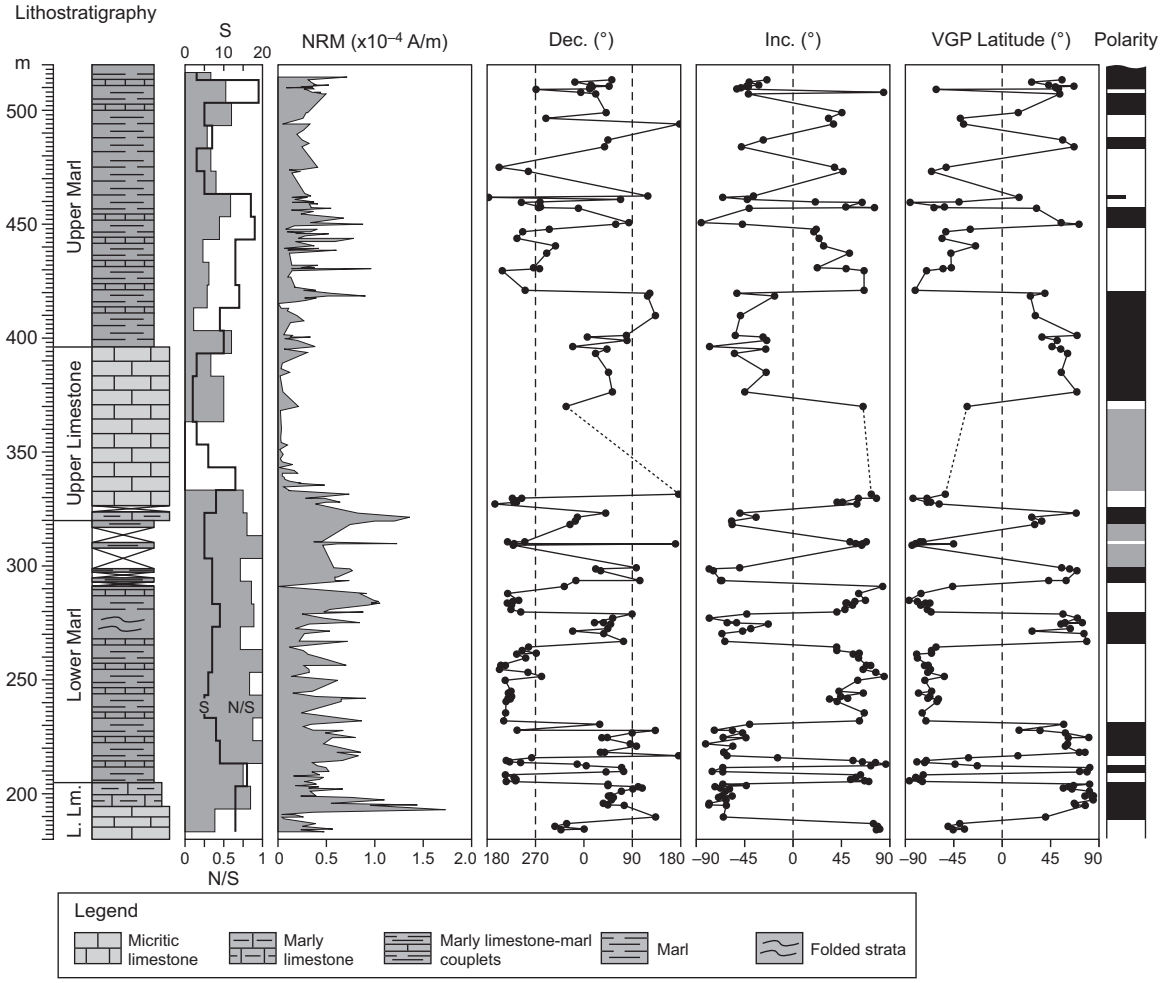

Figure 4. Magnetic polarity stratigraphy of the Mead Stream section. From left to right: Lithostratigraphy; number of demagnetized specimens (*S*, black line) and ratio of the number of characteristic remanent magnetization (ChRM) directions determined (*N*) on the total number of specimens demagnetized (*N*/*S*, gray area); intensity of the natural remanent magnetization (NRM); declination (Dec.) and inclination (Inc.) of the ChRM directions (in tilt-corrected coordinates); derived virtual geomagnetic pole (VGP) latitude and interpreted magnetic polarity stratigraphy; black (white) bands represent normal (reverse) magnetic polarity; gray bands are uncertain polarity zones.

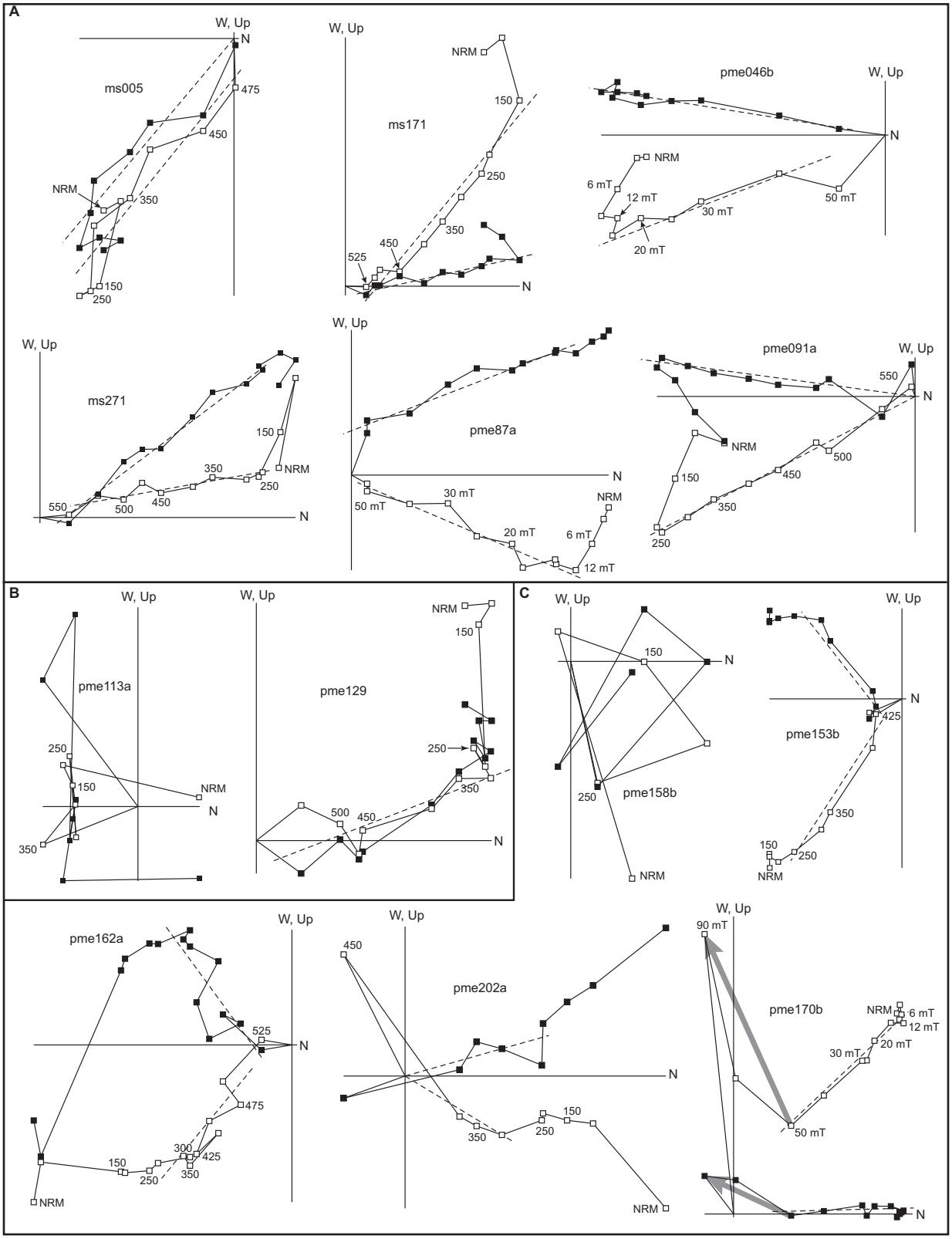

Figure 5. Representative vector end-point demagnetization diagrams for thermally and alternating field (AF) demagnetized specimens (in geographic coordinates); demagnetization steps without units are in °C; black (white) squares represent projections onto the horizontal (vertical) plane; dashed lines highlight the characteristic remanent magnetization (ChRM) component; thick gray arrows indicate the effect of gyroremanent magnetization (GRM), for specimen pme170b. The specimens are subdivided according to lithostratigraphic provenience: (A) Lower Limestone and Lower Marl; (B) Upper Limestone; and (C) Upper Marl. NRM—natural remanent magnetization.

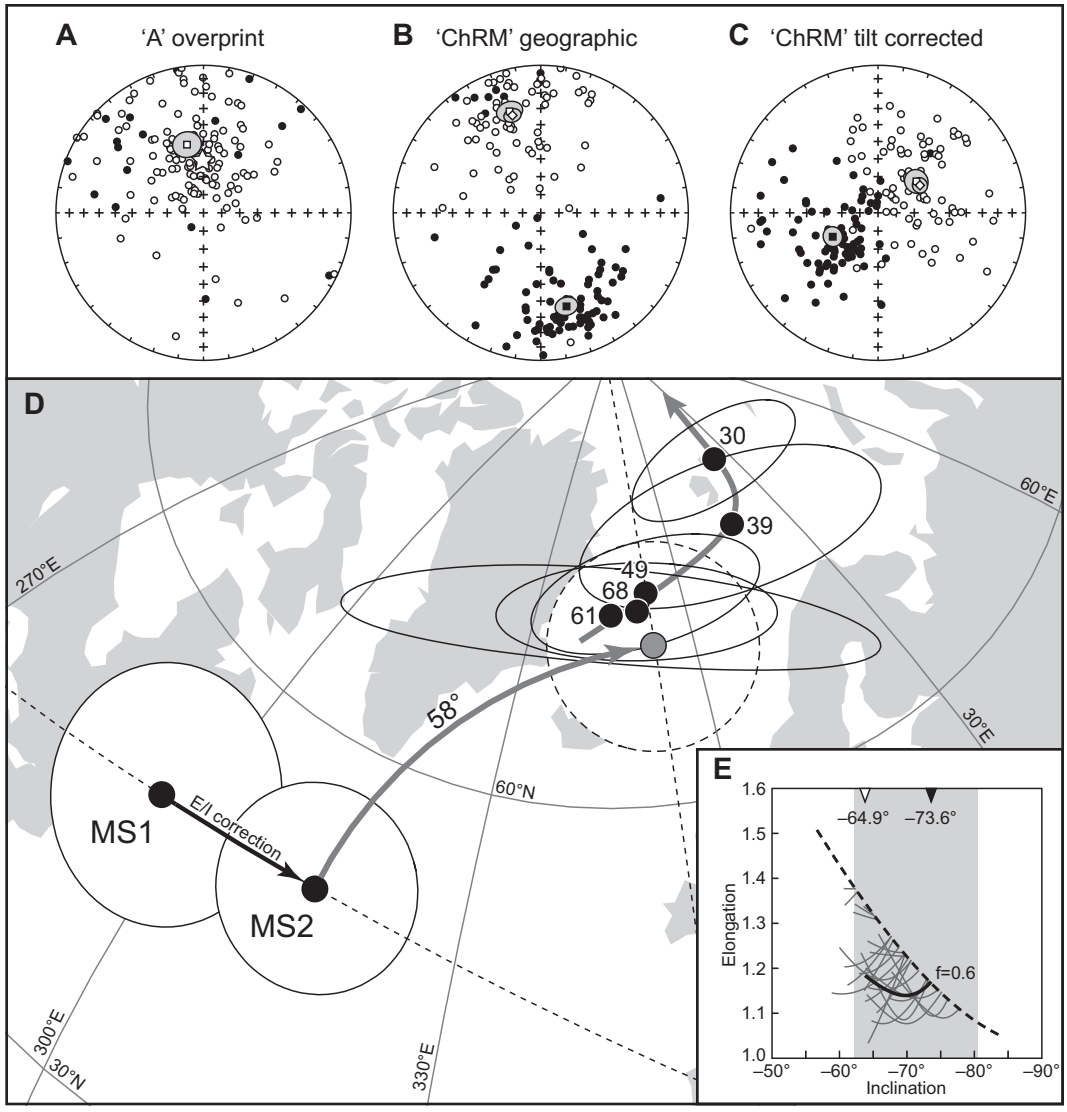

Figure 6. (A) Equal-area projection of the "A" component of the natural remanent magnetization (NRM); white (black) data represent up-pointing (down-pointing) directions; the white square is the average direction, shown with the associated α_{95} cone of confidence (gray circle); the white star represents the direction of geocentric axial dipole (GAD) field at the site latitude. (B) Characteristic remanent magnetization (ChRM) directions from the Mead Stream section in geographic coordinates; up- and down-pointing directions are as in A; the white (black) square is the average direction of the north-and-up (south-and-down) mode, while the white diamond is the average direction obtained inverting all directions to a north-and-up mode; all the average directions are shown with the associated α_{95}. (C) ChRM directions are shown in tilt-corrected coordinates; the average directions and associated confidence boundaries are listed in Table 1. (D) Paleomagnetic pole from the Mead Stream section calculated from a set of 84 ChRM directions with maximum angular deviation (MAD) <7° (MAD_7 directions) before (MS1) and after (MS2) correction for inclination shallowing; the two poles are compared with the reference Paleocene–Oligocene apparent polar wander path (APWP) for the Pacific plate of Beaman et al. (2007), with indication of the age (Ma) associated with each pole; map was drawn with PaleoMac (Cogné, 2003). (E) Elongation vs. inclination (E/I) for the systematically unflattened ChRM directions with the flattening factor *f* (black line) ranging from 1.0 to 0.6, i.e., values at which E/I is found to be consistent with the TK03.GAD geomagnetic field model (dashed line); in order to determine the confidence boundaries (gray band), the analysis has been repeated with a 5000 bootstrapped data set, 25 of which are shown by the gray lines; white (black) triangles are the average inclinations for the MAD_7 directions before (after) E/I correction.

of these specimens underwent erratic increases of magnetization after heating above 400 °C (Fig. 5C, pme202a), associated with the formation of magnetite, likely from a smectite precursor during heating in air (see above).

The ChRM directions are bipolar and oriented NNW-and-up or SSW-and-down in geographic (in situ) coordinates (Fig. 6B; Table 1). After correction for generally homoclinal bedding tilt (mean azimuth of dip/angle of dip = 310°N/62°, except for a few folded strata between 270 and 320 m, for which a local bedding correction was applied), the bipolar ChRM directions become oriented NE-and-up or SW-and-down (Fig. 6C; Table 1). The average directions of the two tilt-corrected modes depart from antipodality by 3.8° and pass the reversal test of Watson (1983; V_w = 1.7, $V_{critical}$ = 6.1; see also Tauxe, 2010) with a class "A" of McFadden and McElhinny (1990). After inverting all ChRM directions to common polarity, we obtained a tilt-corrected mean direction of Dec. = 56.7°, Inc. = –62.2° (N = 158, k = 8.1, α_{95} = 4.2; Fig. 6C; Table 1).

We selected 84 ChRM directions with a maximum angular deviation (MAD) < 7° (MAD_7 directions), which also pass the reversal test (V_w = 0.9, $V_{critical}$ = 6.1), and we determined the mean paleomagnetic pole position of the Mead Stream section by averaging the virtual geomagnetic poles (VGPs) calculated from the MAD_7 directions (MS1 pole; Fig. 6D; Table 1). It is well known that sedimentary rocks can be affected by paleomagnetic inclination flattening errors of different magnitude depending on the magnetic carrier and the degree of postdepositional compaction (e.g., King, 1955; Tauxe and Kent, 1984; Anson and Kodama, 1987; Tan et al., 2002). We used the MAD_7 directions to detect and correct for inclination shallowing by using the

TABLE 1. ChRM DIRECTIONS AND PALEOMAGNETIC POLES FROM THE MEAD STREAM SECTION

		Geographic (in situ) coordinates				Bedding (tilt-corrected) coordinates				
N	MAD	*k*	α_{95}	Dec.	Inc.	*k*	α_{95}	Dec.	Inc.	Inc.*
Normal polarity directions										
79	9.0 ± 6.5	6.8	6.6	344.8	–28.7	7.0	6.5	50.6	–62.5	—
Reverse polarity directions										
79	7.0 ± 4.3	9.9	5.3	166.3	34.9	9.7	5.4	242.3	61.6	—
Reverse and normal polarity directions										
158	8.0 ± 5.7	8.0	4.2	345.6	–31.9	8.1	4.2	56.7	–62.2	—
Reverse and normal polarity MAD_7 directions										
84	4.2 ± 1.7	7.2	6.2	344.4	–32.9	7.4	6.1	58.5	–64.9	$-73.6^{-80.5}_{-62.2}$
Paleomagnetic pole MS1						Paleomagnetic pole MS2				
N	*K*	A_{95}	Long.	Lat.		*K*	A_{95}	Long.	Lat.	
84	4.5	8.2	296.2	49.9		6.5	6.6	314.7	50.7	

Note: ChRM—characteristic remanent magnetization; *N*—number of directions; MAD—maximum angular deviation (°); *k* and K—Fisher (1953) precision parameter of the mean paleomagnetic directions and poles, respectively; α_{95} and A_{95}—Fisher (1953) confidence angle for the mean paleomagnetic directions and poles, respectively; Dec. and Inc.—declination and inclination of paleomagnetic mean directions before and after (*) inclination shallowing correction; Long. and Lat.—longitude and latitude of the paleomagnetic pole before (MS1) and after (MS2) inclination shallowing correction.

elongation/inclination (E/I) method of Tauxe and Kent (2004). This method consists of progressively unflattening the directions by decreasing the flattening parameter *f* (King, 1955) within the formula $\tan I_f = f \cdot \tan I_0$ (where I_f and I_0 are the measured inclination and the true inclination of the geomagnetic field during sedimentation, respectively) until the set of directions assumes an E/I pair of values that is consistent with the TK03.GAD field model (Tauxe and Kent, 2004; Tauxe, 2005). The E/I method has been successfully applied to several deposits of different age (e.g., Kent and Tauxe, 2005; Dallanave et al., 2009, 2012; Muttoni et al., 2013). The analysis was made with L. Tauxe's PmagPy freeware package. The distribution of MAD_7 directions matches the TK03.GAD–predicted E/I values by applying a flattening factor $f = 0.6$, which is in agreement with similar clay-rich calcareous sedimentary facies from the Belluno Basin (Agnini et al., 2011). The corrected mean inclination is –73.6°, i.e., 8.7° steeper than the observed mean inclination (Fig. 6E; Table 1).

We applied a flattening factor of 0.6 to all MAD_7 directions and recalculated the VGPs, which we then averaged to obtain a flattening-free paleomagnetic pole position (MS2; Fig. 6D).

The shallow bias–corrected MS2 paleopole results are displaced by 58° clockwise relative to the ca. 49 Ma reference pole from the Pacific plate apparent polar wander path of Beaman et al. (2007). A post-Eocene clockwise rotation of Mead Stream is in general agreement with the rotations observed in other localities of the Marlborough region (Little and Roberts, 1997; Randall et al., 2011).

Magnetic Polarity Stratigraphy

We used the latitude of the VGP calculated from all the ChRM directions, relative to the mean paleomagnetic (north) pole axis, to interpret magnetic polarity stratigraphy (Lowrie and Alvarez, 1977; Kent et al., 1995). Relative VGP latitudes approaching 90°N and 90°S are interpreted as recording normal and reverse magnetic polarity, respectively. The declination, inclination, and associated VGP latitudes of each ChRM direction are shown in Figure 4. The Mead Stream section records a series of 22 magnetic polarity zones. The integration with the biostratigraphic data allows us to correlate all magnetic zones with the GPTS12 except for the two-sample–based normal polarity interval at ~485.5 m, interpreted as of secondary origin (see below).

Calcareous Nannofossil Biostratigraphy

Calcareous nannofossil preservation is highly variable, with poor preservation usually coinciding with intervals of low abundances. An exception is represented by the basal part of Upper Marl, where low abundance of calcareous nannofossil is associated with moderate preservation. In general, calcareous nannofossil abundance shows large variations throughout the section. In the basal part, across the Lower Limestone and Lower Marl, calcareous nannofossils are characterized by an apparently random alternation between barren to semibarren samples and samples with high abundance. Up section, across the Upper Limestone, calcareous nannofossils are virtually absent. The lack of age-diagnostic taxa limits the application of biostratigraphic schemes. In the upper part of the section, within the Upper Marl, calcareous nannofossils are never abundant, likely due to dilution of the terrigenous component, but they are always present. A further general increase in abundance is observed at the top of the section.

The main biostratigraphic results are reported in stratigraphic order, from oldest to youngest (Fig. 2), and are discussed in relation to the zonation schemes of Martini (1971), Okada and Bukry (1980), and Agnini et al. (2014) (Table A1).

Top Fasciculithus richardii *Group*

Extinction of the *Fasciculithus richardii* group defines the base of zone CNE1 (Agnini et al., 2014). This biohorizon may coincide with the rapid decrease of *Fasciculithus* spp. reported by Hollis et al. (2005a). If this is the case, the position of the base of zone CNE1 is at 154.30 ± 0.3 m, slightly below the onset of the Paleocene Eocene thermal maximum.

Base Rhomboaster *spp. and* Discoaster araneus

The first appearance of *Rhomboaster* spp. defines subzone CP8b (Okada and Bukry, 1980). The concurrent appearances of *Rhomboaster* spp. and *D. araneus* are used to mark the base of subzone NP9b (Aubry et al. 2000). Available data from the literature suggest that B of *Rhomboaster* spp. occurs close to B of *D. araneus* in the earliest Eocene (e.g., Agnini et al., 2007). At Mead Stream, *Rhomboaster* spp. have not been observed, but Hollis at al. (2005a) reported B of *D. araneus* at 159.3 ± 0.3 m. This biohorizon is here used to mark the base of subzone NP9b and of zone CP8b.

Base Tribrachiatus bramlettei

The first appearance of *T. bramlettei* defines the base of zone NP10 of Martini (1971). At Mead Stream, this taxon was not found (Hollis et al., 2005a), which prevents a precise identification of the subzone NP9b–zone NP10 boundary. The base of zone NP10 is approximated by T of *Fasciculithus tympaniformis*.

***Top* Fasciculithus tympaniformis**

Extinction of *F. tympaniformis* marks the base of zone CNE2 (Agnini et al., 2014). At Mead Stream, this biohorizon is observed at 166.88 ± 0.3 m; sporadic occurrences characterize the final occurrence of this taxon. Reworked specimens of fasciculiths are found well above this level.

***Base* Discoaster diastypus *and* Tribrachiatus contortus**

The bases of *D. diastypus* and *T. contortus* are used to define the base of subzone CP9a (Okada and Bukry, 1980). At Mead Stream, *T. contortus* was not found, and the presence of *D. diastypus* is observed just above a semi-barren interval at 183.91 ± 0.07 m. The genus *Discoaster* is unusually rare in this section, and the first presence of *D. diastypus* may not represent the real appearance of this species, an hypothesis that is further supported by the anomalous position of B of *D. diastypus* with respect to B of *Tribrachiatus orthostylus*, with the former biohorizon found after the latter (Agnini et al., 2014).

***Base* Tribrachiatus orthostylus**

The appearance of *Tribrachiatus othostylus* is used to define the base of zone CNE3 (Agnini et al., 2014). At Mead Stream, B of *T. orthostylus* is found at 176.66 ± 3.34 m. Despite the large uncertainness in positioning this biohorizon, likely due to a sampling gap, B of *T. orthostylus* turns out to be a fairly good biohorizon, which is consistent with coeval records (see following).

***Top* Tribrachiatus contortus**

The extinction of *T. contortus* defines the base of zones NP11 and CP9b (Martini, 1971; Okada and Bukry, 1980). These zonal boundaries were not determined because of the absence of *T. contortus*. The bases of zones NP11 and CP9b are approximated by B of *Tribrachiatus orthostylus*.

***Base and Base Common of* Discoaster lodoensis**

The appearance of *D. lodoensis* is used to mark the base of zones CNE4, NP12, and CP10 (Martini, 1971; Okada and Bukry, 1980; Agnini et al., 2014). Although the species belonging to genus *Discoaster* have a sporadic presence throughout the section, Bc of *D. lodoensis* was observed at 221.27 ± 0.85 m.

***Base* Coccolithus crassus**

The appearance of *C. crassus* defines the base of zone CP11 (Okada and Bukry, 1980). At Mead Stream, the sporadic occurrence of this taxon prevents any reliable positioning of B of *C. crassus*.

***Top* Tribrachiatus orthostylus**

The extinction of *T. orthostylus* serves as the base of zones CNE5 and NP13 (Martini, 1971; Agnini et al., 2014). *Tribrachiatus orthostylus* goes extinct at 309.82 ± 0.33 m, just below a sampling gap interval. From ~320 to ~400 m, calcareous nannofossils are sporadic, and age-diagnostic taxa are absent, preventing biostratigraphic classification of this part of the section.

***Top* Blackites gladius**

Top of *B. gladius* marks the base of zone NP16 (Martini, 1971). This taxon was not encountered in this study. The base of zone NP16 is approximated by Bc of *Reticulofenestra umbilicus*.

***Base Common* Reticulofenestra umbilicus**

The Bc of *R. umbilicus* defines the base of zone CNE13 and subzone CP14a (Okada and Bukry, 1980; Agnini et al., 2014). Taking into account the low abundance of calcareous nannofossils around 400 m, B of *R. umbilicus*, recorded at Mead Stream at 400.00 ± 0.20 m, may approximate the Bc recorded in more favorable conditions (ODP Site 1051; Agnini et al., 2014).

Base Common* Cribrocentrum reticulatum *(Base of Zone CNE14)

The Bc of *C. reticulatum* marks the base of zone CNE14 (Agnini et al., 2014). At Mead Stream, the first specimens of *C. reticulatum* are found at 440.95 ± 0.45 m, after an interval of virtual absence of calcareous nannofossils; this implies that *C. reticulatum* may be present, although not recorded, also below this level.

***Top* Chiasmolithus solitus**

The T of *Chiasmolithus solitus* defines the bases of zone NP17 and subzone CP14b (Martini, 1971; Okada and Bukry, 1980). At Mead Stream, *C. solitus* has sporadic occurrences up to 479.5 ± 4.5 m. Even if this datum is consistent with abundance patterns from ODP Sites 1052 and 1263 (see following), Fornaciari et al. (2010) showed that this taxon has uneven distribution in other sections. In the presence of alternative biohorizons such as B of *D. bisectus*, we thus discourage the use of T of *C. solitus* as a biomarker.

Base* Dictyococcites bisectus *(Base of Zone CNE15)

The B of *D. bisectus* is used to define the base of zone CNE15 (Agnini et al., 2014). Specimens of *D. bisectus* first enter in the record at 490.40 ± 0.90 m. This datum could serve to approximate the onset of the middle Eocene climatic optimum in the section (Toffanin et al., 2011, 2013).

Foraminiferal Biostratigraphy

Foraminiferal biostratigraphy is used to correlate the Eocene section to New Zealand stages (Fig. 2). The boundary between the Waipawan and Mangaorapan stages is located in the Lower Marl directly below an interval of deformed strata that is roughly estimated to represent 14 m of stratigraphic section (265–279 m). The base of the Mangaorapan stage is recognized by B of *Morozovella crater*, which occurs between 260.9 and 263 m. The base of the Heretaungan stage is uncertainly located in the section because the primary index species, *Elphidium hampdenense*, has not been recognized. A secondary datum, T of *Gaudryina reliqua*, indicates the base of the stage is located in the uppermost part of the Lower Marl (318.12–320.42 m). The base of the Porangan stage is recognized by T of *M. crater*, which is poorly constrained within the highly indurated Upper Limestone to an interval between 334.78 and 375.27 m. An earlier record of an isolated occurrence of the primary index species *Elphidium saginatum* (~345 m) supports placing the base of the stage at this level. The base of the Bortonian stage is also poorly constrained and is recognized by T of *Globigerapsis index* in the upper part of the Upper Limestone between 375.27 and 397 m.

DISCUSSION

Magneto-Biostratigraphic Correlation

We compared the Mead Stream magneto-biostratigraphy with correlative magneto-biostratigraphies from several deep-sea cores and uplifted marginal marine sections (Figs. 1 and 7). These are ODP Sites 1258A, 1260B (Leg 207, Demerara Rise; Edgar et al., 2010; Suganuma and Ogg, 2006), and 1051A (Leg 171b, Blake Nose; Edgar et al., 2010; Ogg and Bardot, 2001) from the Atlantic Ocean, and the on-land Contessa Highway (Lowrie and Alvarez, 1977; Jovane et al., 2007), Possagno (Agnini et al., 2006), Alano (Agnini et al., 2011), and Cicogna (Dallanave et al., 2009) sections from Italy (Tethys Ocean). It is important to note that the magnetostratigraphy of ODP Sites 1258A and 1260B was constructed by comparing the relative angle between the low-temperature magnetic overprint and the higher-temperature ChRM of the sediments (see also Shibuya et al., 1991), a method that does not allow application of standard reliability tests for the paleomagnetic data (e.g., Tauxe et al., 2012).

We obtained an excellent overall magnetic polarity correlation that is supported by a general consistency of the position of calcareous nannofossil biohorizons (Fig. 7). In addition,

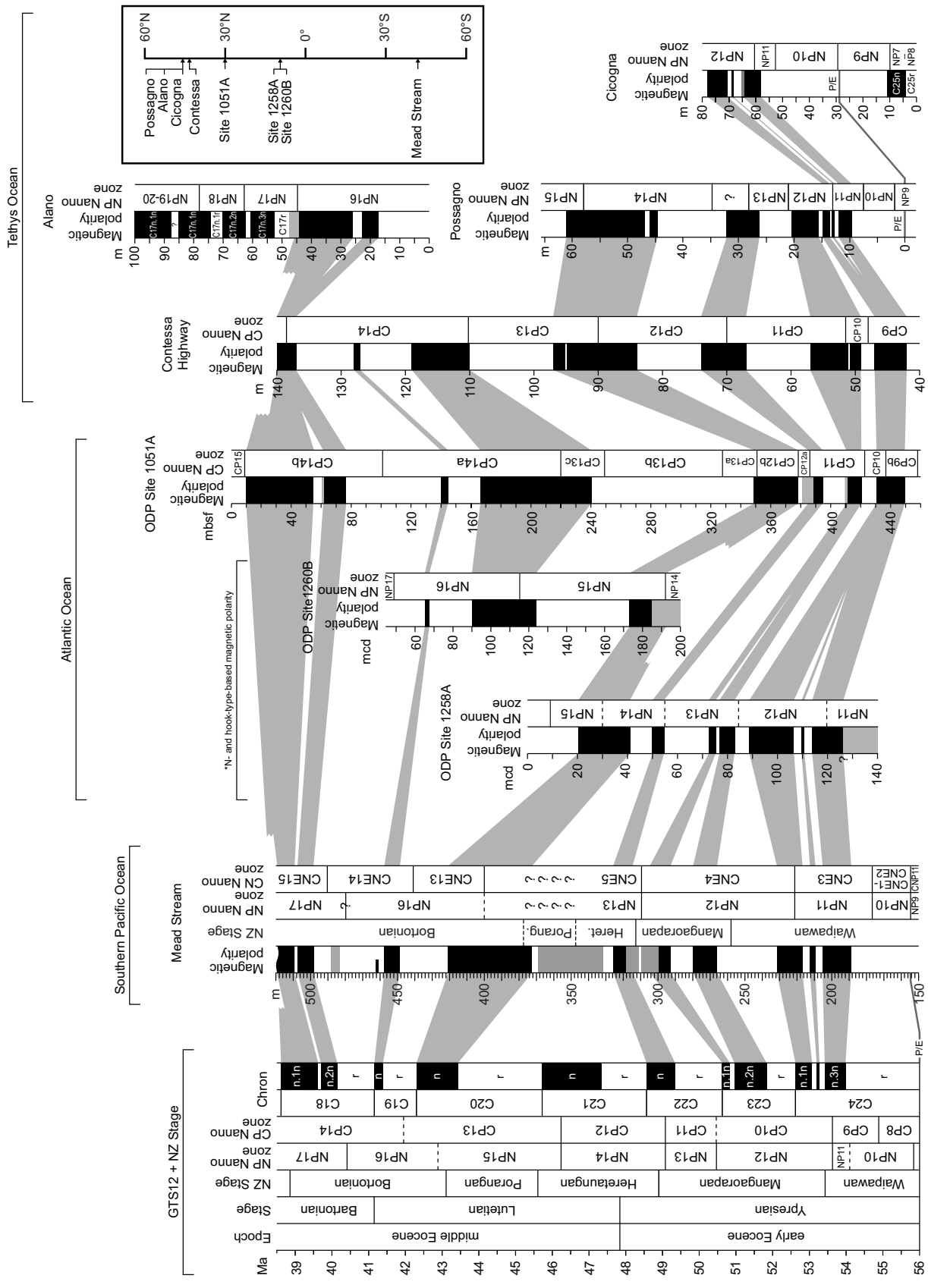

Figure 7. The magneto-biostratigraphy of the Mead Stream section compared with other representative records from the South Pacific Ocean, Atlantic Ocean, and Tethys Ocean domains (references listed in the main text), as well as with the geomagnetic polarity time scale of Gradstein et al. (2012; GTS12) integrated with the New Zealand (NZ) stages calibrated by Hollis et al. (2010); asterisk indicates the magnetic polarity stratigraphy of these sites is based on the shape of the vector–end-point demagnetization diagrams and not on the inclination of the characteristic remanent magnetization as is usual practice. Inset: Present-day latitudinal positions of the records. P/E—Paleocene-Eocene boundary. Calcareous nannofossil zonation is from Martini (1971; NP zones), Okada and Bukry (1980; CP zones), and from Agnini et al. (2014; CN zones); mcd—meter of composite depth; mbsf—meter below sea floor.

comparison with the reference GPTS12 time scale allows correlation of the 22 magnetic polarity intervals found at Mead Stream with chrons C24r to C18n.1n. The stratigraphic levels of the magnetic polarity reversals are listed in Table A1. Integration of the magnetic polarity stratigraphy with calcareous nannofossil and foraminiferal biostratigraphy allows us to establish that chron C21n occurs within the Upper Limestone, which is characterized by extremely low NRM values (Fig. 4) and random demagnetization behavior (Fig. 5B). Furthermore, within this correlation framework, we observe that the two-sample–based normal polarity event found at 485.5 m within chron C18r has no obvious counterpart in any other record, nor can it be successfully correlated with the GPTS. Hence, we provisionally interpret these north-and-up ChRM directions as overprints of diagenetic origin recording a postdepositional field of normal polarity. The part of the Mead Stream section considered here thus spans from ca. 56 Ma (immediately below the Paleocene-Eocene boundary located at 157 m; Hollis et al., 2005a) up to ca.39 Ma. It encompasses 17 m.y. of South Pacific Ocean history from the latest Paleocene to late middle Eocene, calibrated with a robust magnetic polarity record.

Age Model of Sedimentation and Biochronology

We constructed an age-depth plot for the Mead Stream section from the magnetic polarity correlation with the reference GPTS of Ogg and Smith (2012). As chronologic control points, we used the series of 18 magnetic polarity reversals retrieved from the section, straddling from the top of chron C24r to the base of chron C18n.1n (aside from chron C21n, which is not recorded at Mead Stream), integrated with the position of the Paleocene-Eocene boundary at 156.8 m (Hollis et al., 2005a). We derived the sediment accumulation rates (SARs) assuming rates to be constant between age tie-points (Fig. 8).

SARs are ~20 m/m.y. in the Lower Limestone and increase to ~50 m/m.y. within the Lower Marl. The interval between 270 m and 320 m is complicated by folding and faulting. SARs that peak to ~100 m/m.y. across chron C23n.1r, and then drop to 10 m/m.y. across chron C22r, are likely an artifact of this deformation. Relatively low SARs of ~10 m/m.y. are observed for the Upper Limestone. SARs increase again to ~40 m/m.y. within the Upper Marl, and then decrease to ~20 m/m.y. at the top of the unit (Fig. 8).

We assigned the age of the calcareous nannofossil biohorizons using the GPTS12-based age model. Biostratigraphic data of B of *D. araneus* and the rapid decrease in abundance of *Fasciculithus* spp. are from Hollis et al. (2005a). Here, we only present the calibration based on our age model. Instead, from the Paleocene–Eocene thermal maximum upward, calcareous nannofossil biostratigraphic and biochronologic data are from this study.

T of *F. tympaniformis*, B of *T. orthostylus*, and B of *D. diastypus* are correlated with the mid-upper part of chron C24r. Overall, these data are consistent with previous results from low- to midlatitudes (Agnini et al., 2014), even though at Mead Stream, B of *D. diastypus* occurs above B of *T. orthostylus*, rather than below. The apparent inconsistency of this datum is likely due to the extreme rarity of discoasters throughout the section. Bc of *D. lodoensis* and T of *T. orthostylus* lie within chron C24n and chron C22r, respectively, in good agreement with biochronologic data from other mid-latitude sections (Agnini et al., 2014). The lower part of the middle Eocene (Lutetian) is virtually barren in calcareous nannofossils, which implies that no biostratigraphic data are available in the interval between T of *T. orthostylus* and Bc of *R. umbilicus*. In the upper part of the section, Bc of *R. umbilicus*, Bc of C. *reticulatum*, and B of *D. bisectus* are recorded within chrons C20n, C19r, and C18r, respectively. Even though calcareous nannofossils never reach high abundances, biochronologic data are in fair agreement with those obtained from ODP Site 1051, one of the reference sections for this time interval (Agnini et al., 2014).

T of *C. solitus* at Mead Stream lies in the middle part of chron C18r. This datum is consistent with abundance patterns from ODP Sites 1052 and 1263, which have a final common and continuous occurrence within chron C18r (Fornaciari et al., 2010).

The locations of all but one (base of Mangaorapan) of the New Zealand Eocene stage boundaries determined by foraminiferal biostratigraphy are consistent with nannofossil biostratigraphy and magnetostratigraphy (Figs. 7 and 8; Table A1). The base of the Mangaorapan is tied to the base of nannofossil zone NP12 (Hollis et al., 2010). However, at Mead Stream, the base of the stage, defined by B of *M. crater*, lies ~40 m higher (Fig. 7). This delayed appearance of *M. crater* was also noted by Slotnick et al. (2012) and may reflect relatively cool oceanographic conditions in this setting, which may also account for the low abundance of *Discoaster* spp. noted previously. The base of the Heretaungan is tied to the base of nannofossil zone NP14 (Hollis et al., 2010), which occurs at the base of chron C22n (Berggren et al., 1995). This correlation is supported by the record at Mead Stream where the secondary datum for the base of the Heretaungan, T of *G. reliqua*, occurs directly above C22n (Table A1). The base of the Porangan and the Bortonian are not well constrained at Mead Stream. However, the estimated ages of 45.4 Ma and 43.1 Ma, respectively, are in good agreement with recalibrated ages determined from Hollis et al. (2010).

Climate and Sedimentation

We examined the long-term (million-year-scale) effect of climate variations on sedimentation patterns at Mead Stream using the magnetic polarity–based age model of sedimentation. In order to do that, we plotted SARs at Mead Stream on the GPTS12 time scale together with the main lithology subdivisions of the Amuri Limestone (Fig. 9). The highest SARs were observed around 52 Ma during deposition of the Lower Marl, which has an average terrigenous content of ~35% (Fergusson, 1985; Morris, 1987). The SARs drop to minimum values between ca. 49 Ma and 44 Ma during deposition of the Upper Limestone, which are well-indurated limestones with a terrigenous content <10% (Fergusson, 1985; Morris, 1987). Then, SARs increase again, together with the terrigenous content of the sediments (~30%; Fergusson, 1985; Morris, 1987), during deposition of the Upper Marl from 44 Ma up to ca. 40 Ma. In this context, we interpreted the higher SARs observed across the Lower and Upper Marl as the result of two long-term intervals of increased physical weathering related to warm and humid climatic optima.

To verify this hypothesis, we compared SARs from Mead Stream with the South Pacific TEX_{86} marine temperature proxy records from the mid-Waipara River section (Hollis et al., 2009) and from ODP Site 1172 (Leg 189, East Tasman Plateau; Bijl et al., 2009), as well as with the multi-site composite benthic $\delta^{18}O$ record of Zachos et al. (2008; recalibrated to the GPTS12). The early Eocene high SARs correlate with the early Eocene climatic optimum, centered at ca. 52 Ma, which was the warmest time period of the Cenozoic (e.g., Zachos et al., 2001, 2008). The early Eocene climatic optimum was followed through the early–middle Eocene by a global cooling trend, which correlates with the lowest SARs registered across the section between ca. 49 and 44 Ma. From ca. 44 Ma to 40 Ma, the $\delta^{18}O$ proxy data indicate a transient return to warmer climate conditions that peaked at ca. 40.5 Ma with the middle Eocene climatic optimum (Bohaty and Zachos, 2003; Bohaty et al., 2009), which correlates with a subsequent increase in SARs.

This correlation indicates that early to middle Eocene climate evolution had an active role in deposition of the Amuri Limestone: times

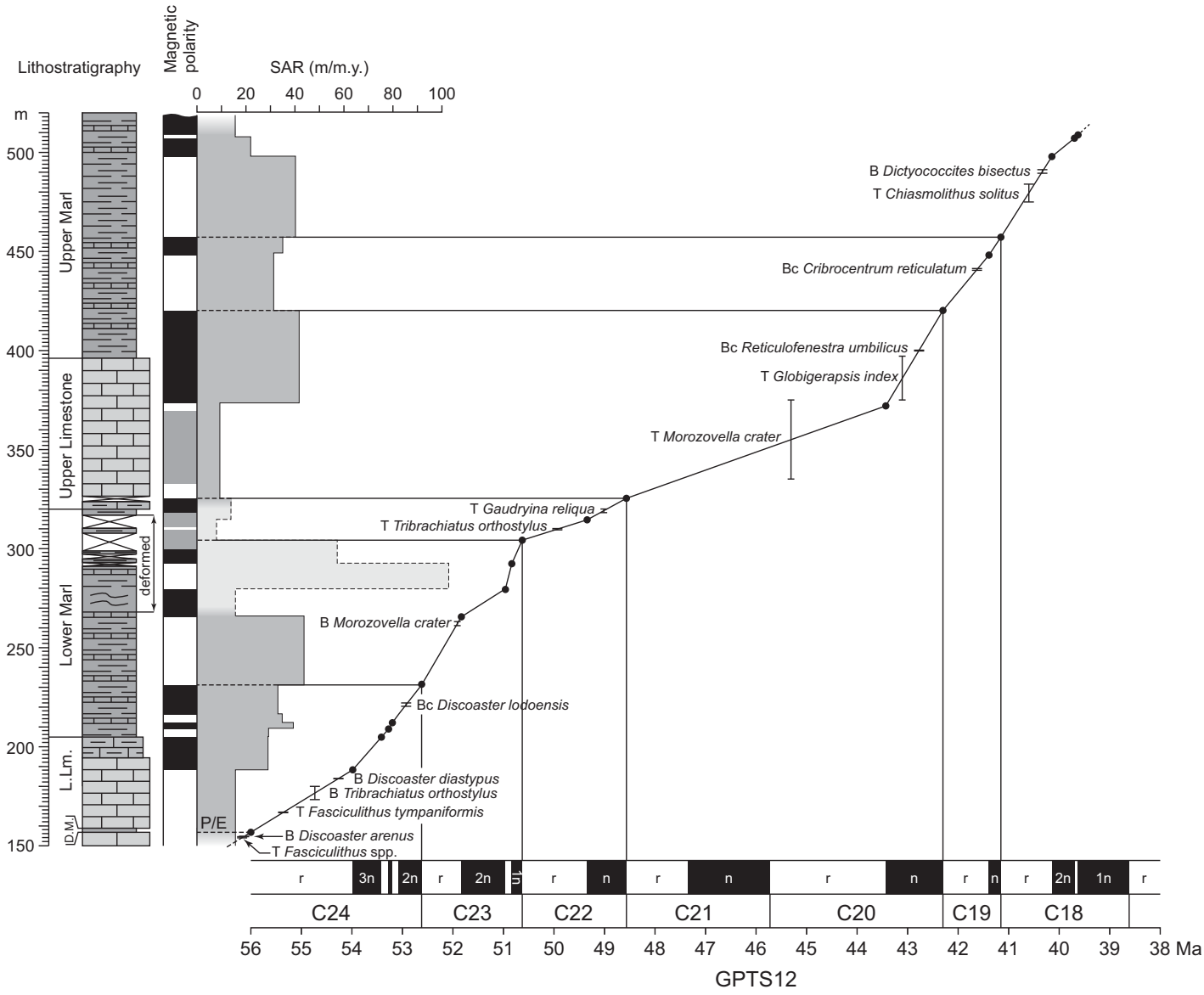

Figure 8. Age-depth model and derived sediment accumulation rates (SARs) for the Mead Stream section (L. Lm.—Lower Limestone; D.M.—Dee marl) obtained by magnetostratigraphic correlation to the geomagnetic polarity time scale of Ogg and Smith (2012; GPTS12). Key calcareous nannofossil and foraminiferal biohorizons are also indicated (B—base, Bc—base common, T—top). The light-gray SAR zones bounded by the dashed line highlight the unreliable values obtained across faulted and folded strata between 280 and 320 m. See figure 2 for the lithology legend.

with warmer climates were characterized by an enhanced hydrological cycle that promoted continental weathering on land, followed by the transport and deposition of terrigenous sediments in adjacent basins. This line of argument is in agreement with Slotnick et al. (2012), who interpreted the marl-rich horizons and intervals of the Lower Limestone and Lower Marl as reflecting an accelerated hydrological cycle with enhanced seasonality, especially during the warmer background conditions of the early Eocene climatic optimum in the Lower Marl. This interpretation integrates concepts derived from climate model simulations that predict enhancement of the hydrological cycle and river discharge, associated at mid-latitudes with greater seasonal precipitation as a consequence of climate warming (Peterson et al., 2002; Murphy et al., 2004; Held and Soden, 2006; Meehl et al., 2007a, 2007b). Our correlation of the Mead Stream SARs with the global climate proxy record also confirms the hypothesis of Slotnick et al. (2012), i.e., that the transition from the Lower Marl to Upper Limestone marks the end of the early Eocene climatic optimum, while the Upper Marl represents a return to an enhanced terrigenous discharge on a seasonal basis.

The presence of smectite as the dominant clay mineral in the terrigenous fraction of the Mead Stream sediment (Fergusson, 1985; Morris, 1987) also seems to indicate enhanced chemical weathering. This is because smectite is a common weathering product formed under warm and humid (tropical-type) climate conditions (Fagel, 2007). A million-year-scale correlation between climate and clay content of sediments is in agreement with Thiry (2000), who predicted a resolution of the

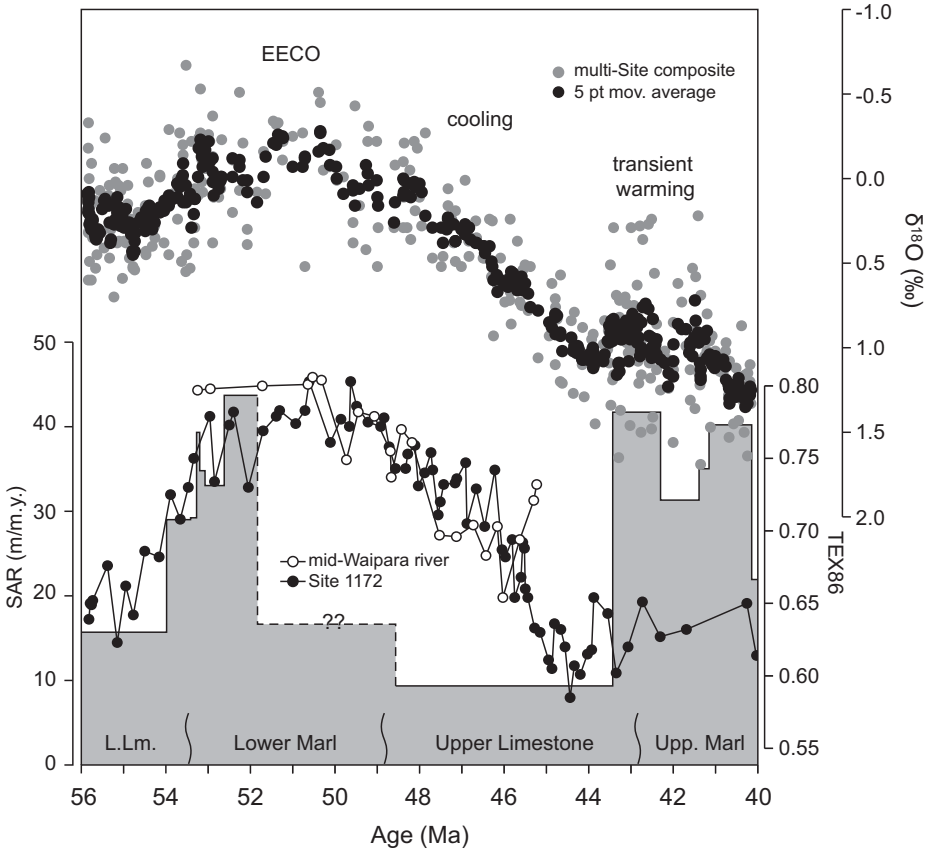

Figure 9. Sediment accumulation rates (SARs; gray area) compared with the TEX_{86} record from Ocean Drilling Program (ODP) Site 1172 and from the mid-Waipara River section (Bijl et al., 2009; Hollis et al., 2009) as well as with the benthic oxygen isotope ($\delta^{18}O$) records of Zachos et al. (2008; global ocean) plotted on the geomagnetic polarity time scale of Gradstein et al. (2012). See text for details. EECO—early Eocene climatic optimum.

paleoclimatic record in marine clay not shorter than 1–2 m.y.

Enhanced formation, transportation, and sedimentation of smectite during early–middle Eocene warmer times are consistent with the shift from smectite-dominated assemblages to illite- and chlorite-dominated assemblages observed in earliest Oligocene sediments of the Pacific sector of the Antarctic Ocean (McMurdo Sound, Ross Sea, Antarctica), which is interpreted as reflecting the transition from chemical weathering conditions under warm and humid Eocene climates to physical weathering under cooler conditions typical of the Oligocene (Ehrmann et al., 1992, 2005; Ehrmann, 2001). At the same location, evidence has also been found of a million-year-scale temporary increase of smectite content, driven by transient warming, in late Eocene sediments (Sagnotti et al., 1998; Roberts et al., 2013b). Enhanced chemical weathering parallel to climate warming is in agreement with the climate-buffering negative feedback via sequestration of atmospheric CO_2 on land through the weathering of Fe- and Mg-silicates (followed by carbonate deposition) first proposed by Walker et al. (1981). This mechanism controls how much CO_2 is retained in the atmosphere (Kent and Muttoni, 2013), thus modulating long-term climate variability. However, we cannot exclude an authigenic origin for smectite, which in deep-sea sediment can derive from several processes (e.g., Bohrmann and Thiede, 1989). For example, authigenic smectite has been observed in Cretaceous deep-sea sediments from the Atlantic Ocean (Thiry and Jacquin, 1993), formed by transformation and recrystallization of detrital material during early diagenesis.

CONCLUSIONS

The Mead Stream section represents the most complete, continuous, and expanded magneto-biostratigraphically calibrated sedimentary record deposited on a continental shelf during the early to middle Eocene in the South Pacific Ocean. Our studied interval includes the interval from the Paleocene-Eocene boundary at 56 Ma to chron C18n.1n at ca. 39 Ma, encompassing 17 m.y. of South Pacific Ocean history from the Ypresian to the Bartonian, i.e., from the Waipawan to the Bortonian New Zealand stages. The ages of calcareous nannofossil biohorizons estimated at Mead Stream are consistent with recently published data from low- to mid-latitude sequences. We therefore conclude that during the early–middle Eocene, the Mead Stream section belonged to the low- to mid-latitude paleobiogeographic domain. These data provide the first independent biochronology obtained by direct calibration of calcareous nannofossil biohorizons and magnetostratigraphy from the South Pacific, a crucial area for understanding early Paleogene climate and biotic evolution.

We used our robust new age model to investigate the correlation between climate and sedimentation at Mead Stream, whereby the global warming events of the early–middle Eocene are characterized by increased SARs, which indicate enhanced terrigenous input related to increased hydrological cycle. The presence of smectite in the clay-rich sediments of the Lower Marl and Upper Marl, where the SARs are higher, possibly indicates also increased continental chemical weathering, in agreement with the negative feedback mechanism to buffer CO_2 variations of the ocean-atmosphere reservoir through the weathering of silicates (Walker et al., 1981). To find evidence of this mechanism in the geological past, several proxies have been proposed that register ocean chemistry changes derived from continental weathering variations. These include variations in radiogenic isotope ratios (e.g., $^{87}Sr/^{86}Sr$, $^{187}Os/^{188}Os$), bulk phosphorous burial (Föllmi, 1995), and other elemental ratios (see Kump et al., 2000). Most of these proxies represent average readings of different inputs, and whether they faithfully record changes in weathering fluxes remains open to question. An alternative approach has been proposed by Dallanave et al. (2010). By studying the early Eocene sediments of the Belluno Basin (NE Italy), they found that global warming culminating with the early Eocene climatic optimum was characterized by relative increases of more-oxidized detrital Fe-minerals, which are interpreted as derived by enhanced chemical weathering on land, whereas during pre–early Eocene climatic optimum cooler climates, sediments were proportionally enriched in less-oxidized detrital phases. SAR variations at Mead Stream, in association with the presence of smectite, represent a sedimentological proxy to confirm the existence of this negative feedback mechanism during the early–middle Eocene.

APPENDIX

Table A1. List and position of biostratigraphic events and lower magnetic polarity Chron boundaries for the Mead Stream section.

TABLE A1. LIST AND POSITION OF BIOSTRATIGRAPHIC EVENTS AND LOWER MAGNETIC POLARITY CHRON BOUNDARIES FOR THE MEAD STREAM SECTION

Event or chron base	Biozone (NZ stage) base	Sample base (m)	Sample top (m)	Mean position (m)	Error (m)	Chron	Fractional position from top chron	Age (Ma, GPTS12)	
C18n.1n		507.90	509.40	508.65	0.75				
C18n.1r		507.20	507.90	507.55	0.35				
C18n.2n		496.50	499.00	497.75	1.25				
B *Dictyococcites bisectus*	CNE15	489.50	491.30	490.40	0.90	C18r	0.18	40.33	
T *Chiasmolithus solitus (?)*	NP17/CP14b	475.00	484.00	479.50	4.50	C18r	0.45	40.60	
C18r		457.00	457.30	457.15	0.15				
C19n		447.80	450.00	448.90	1.10				
Bc *Cribrocentrum reticulatum*	CNE14	440.50	441.40	440.95	0.45	C19r	0.28	41.64	
C19r		419.70	421.00	420.35	0.65				
Bc *Reticulofenestra umbilicus*	CNE13	399.80	400.20	400.00	0.20	C20n	0.43	42.79	
T *Globigerapsis index*	Bortonian	375.27	397.00	386.14	10.87	C20n	0.73	43.11	
C20n		370.00	376.40	373.20	3.20				
B *Elphidium saginatum*		345.00	345.00	345.00	—	C20r(?)	—	46.44	
T *Morozovella crater*	Porangan	334.78	375.27	355.03	20.25	C20r(?)	—	45.37	
C21r		323.20	327.20	325.20	2.00				
T *Gaudryina reliqua*	Heretaungan	318.12	320.42	319.27	1.15	C22n	0.55	48.98	
C22n		310.60	318.20	314.40	3.80				
T *Tribrachiatus orthostylus*	CNE5	309.48	310.15	309.82	0.33	C22r	0.45	49.92	
C22r		299.20	309.10	304.15	4.95				
C23n.1n		291.00	293.60	292.30	1.30				
C23n.1r		278.90	279.80	279.35	0.45				
C23n.2n		264.40	266.90	265.65	1.25				
B *Morozovella crater*	Mangaorapan	260.90	263.00	261.95	1.05	C23r	0.11	51.91	
C23r		230.50	232.00	231.25	0.75				
Bc *Discoaster lodoensis*	CNE4	220.42	222.12	221.27	0.85	C24n.1n	0.67	52.92	
C24n.1n		215.80	216.70	216.25	0.45				
C24n.1r		211.50	212.30	211.90	0.40				
C24n.2n		208.30	209.60	208.95	0.65				
C24n.2r		204.20	205.40	204.80	0.60				
C24n.3n		186.90	189.80	188.35	1.45				
B *Discoaster diastypus*	CP9a	183.83	183.98	183.91	0.07	C24r		54.26	*
B *Tribrachiatus orthostylus*	CNE3	173.32	180.00	176.66	3.34	C24r		54.72	*
T *Fasciculithus tympaniformis*	CNE2	166.72	167.03	166.88	0.16	C24r		55.33	*
Paleocene-Eocene boundary		156.40	157.20	156.80	0.40	C24r		55.96	*
B *Discoaster araneus*	NP9b	154.60	154.80	154.70	0.10	C24r		56.09	*
T *Fasciculithus* spp. (?)	CN1?	154.00	154.60	154.30	0.30	C24r		56.12	*
CN zone (Agnini et al., 2014)									
NP zone (Martini, 1971)									
CP zone (Okada and Bukry, 1980)									

Note: Ages of bioevents were calculated by means of correlation of the magnetostratigraphy with the geomagnetic polarity time scale of Ogg and Smith (2012; GPTS12).

*Ages of biohorizons within chron C24r were calibrated using the age of the Paleocene-Eocene thermal maximum (55.96 Ma; GTS12) as additional tie point.

ACKNOWLEDGMENTS

We thank the Murray family for permitting us access to the Mead Stream section. We are grateful to Andrew P. Roberts and Gerald R. Dickens for comments that greatly improved the quality of this manuscript. This study was financed by grant Ba1210/19-1 and 19-2 of the Deutsche Forschungsgemeinschaft (DFG) to Bachtadse and the Government of New Zealand through the GNS Science Global Change through Time Program (540GCT62)

REFERENCES CITED

Agnini, C., Muttoni, G., Kent, D.V., and Rio, D., 2006, Eocene biostratigraphy and magnetic stratigraphy from Possagno, Italy: The calcareous nannofossil response to climate variability: Earth and Planetary Science Letters, v. 241, p. 815–830, doi:10.1016/j.epsl.2005.11.005.

Agnini, C., Fornaciari, E., Raffi, I., Rio, D., Röhl, U., and Westerhold, T., 2007, High-resolution nannofossil biochronology of middle Paleocene to early Eocene at ODP Site 1262: Implications for calcareous nannoplankton evolution: Marine Micropaleontology, v. 64, p. 215–248, doi:10.1016/j.marmicro.2007.05.003.

Agnini, C., Fornaciari, E., Giusberti, L., Grandesso, P., Lanci, L., Luciani, V., Muttoni, G., Pälike, H., Rio, D., Spofforth, D.J.A., and Stefani, C., 2011, Integrated biomagnetostratigraphy of the Alano section (NE Italy): A proposal for defining the middle-late Eocene boundary: Geological Society of America Bulletin, v. 123, p. 841–872, doi:10.1130/B30158.1.

Agnini, C., Fornaciari, E., Raffi, I., Catanzariti, R., Pälike, H., Backman, J., and Rio, D., 2014, Biozonation and biochronology of Paleogene calcareous nannofossils from low and middle latitudes: Newsletters on Stratigraphy, v. 47, p. 131–181, doi:10.1127/0078-0421/2014/0042.

Anson, G., and Kodama, K., 1987, Compaction-induced inclination shallowing of the post-depositional remanent magnetization in a synthetic sediment: Geophysical Journal of the Royal Astronomical Society, v. 88, p. 673–692, doi:10.1111/j.1365-246X.1987.tb01651.x.

Aubry, M.-P., 1984, Handbook of Cenozoic Calcareous Nannoplankton, book 1. Ortholithae (Discoaster): New York, American Museum of Natural History Micropaleontology Press, 263 p.

Aubry, M.-P., 1988, Handbook of Cenozoic Calcareous Nannoplankton, book 2. Ortholithae (Catinasters, Ceratoliths, Rhabdoliths): New York, American Museum of Natural History Micropaleontology Press, 279 p.

Aubry, M.-P., 1989, Handbook of Cenozoic Calcareous Nannoplankton, book 3. Ortholithae (Pentaliths and Other), Heliolithae (Fasciculiths, Sphenoliths and Others): New York, American Museum of Natural History Micropaleontology Press, 279 p.

Aubry, M.-P., 1990, Handbook of Cenozoic Calcareous Nannoplankton, book 4. Heliolithae (Helicoliths, Cribriliths, Lopadoliths and Others): New York, American Museum of Natural History Micropaleontology Press, 381 p.

Aubry, M.-P., 1999, Handbook of Cenozoic Calcareous Nannoplankton. Heliolithae (Zygoliths and Rhabdoliths): New York, American Museum of Natural History Micropaleontology Press, 368 p.

Aubry, M.-P-, Cramer, B.S., Miller, K.G., Wright, J.D., Kent, D.V., and Olsson, R.K., 2000, Late Paleocene event chronology: unconformities, not diachrony: Bulletin de la Societe Geologique de France, v. 171, no. 3, p. 367–378.

Backman, J., and Shackleton, N., 1983, Quantitative biochronology of Pliocene and Early Pleistocene calcareous nannofossils form the Atlantic, Indian and Pacific Ocean: Marine Micropaleontology, v. 8, p. 141–170.

Backman, J., Raffi, I., Rio, D., Fornaciari, E., and Pälike, H., 2012, Biozonation and biochronology of Miocene through Pleistocene calcareous nannofossils from low and middle latitudes: Newsletters on Stratigraphy, v. 45, p. 221–244, doi:10.1127/0078-0421/2012/0022.

Bains, S., 1999, Mechanisms of climate warming at the end of the Paleocene: Science, v. 285, p. 724–727, doi:10.1126/science.285.5428.724.

Ballance, P.F., 1993, The paleo-Pacific, post-subduction, passive margin thermal relaxation sequence (Late Cretaceous–Paleogene) of the drifting New Zealand continent, *in* Ballance, P.F., ed., Sedimentary Basins of the World, Volume 2: South Pacific Sedimentary Basins: Amsterdam, Netherlands, Elsevier, p. 93–110.

Beaman, M., Sager, W., Acton, G., Lanci, L., and Pares, J., 2007, Improved Late Cretaceous and early Cenozoic paleomagnetic apparent polar wander path for the Pacific plate: Earth and Planetary Science Letters, v. 262, p. 1–20, doi:10.1016/j.epsl.2007.05.036.

Berggren, W.A., Kent, D.V., Swisher, C.C., III, and Aubry, M.-P., 1995, A revised Cenozoic geochronology and chronostratigraphy, *in* Berggren, W.A., Kent, D.V., Aubry, M.-P., and Hardenbol, J., eds., Geochronology, Time Scales and Global Stratigraphy Correlation: A Unified Temporal Framework for a Historical Geology: Society of Economic Paleontologists and Mineralogists Special Publication 54, p. 129–213.

Bijl, P.K., Schouten, S., Sluijs, A., Reichart, G.-J., Zachos, J.C., and Brinkhuis, H., 2009, Early Palaeogene temperature evolution of the southwest Pacific Ocean: Nature, v. 461, p. 776–779, doi:10.1038/nature08399.

Bijl, P.K., Bendle, J.A., Bohaty, S.M., Pross, J., Schouten, S., Tauxe, L., Stickley, C.E., McKay, R.M., Röhl, U., Olney, M., Sluijs, A., Escutia, C., and Brinkhuis, H., 2013, Eocene cooling linked to early flow across the Tasmanian Gateway: Proceedings of the National Academy of Sciences of the United States of America, v. 110, p. 9645–9650, doi:10.1073/pnas.1220872110.

Bohaty, S.M., and Zachos, J.C., 2003, Significant Southern Ocean warming event in the late middle Eocene: Geology, v. 31, p. 1017–1020, doi:10.1130/G19800.1.

Bohaty, S.M., Zachos, J.C., Florindo, F., and Delaney, M.L., 2009, Coupled greenhouse warming and deep-sea acidification in the middle Eocene: Paleoceanography, v. 24, PA2207, doi:10.1029/2008PA001676.

Bohrmann, G., and Thiede, J., 1989, Diagenesis in Eocene claystones, ODP Site 647, Labrador Sea: Formation of complex authigenic carbonates, smectites, and apatite, *in* Srivastava, S.P., Arthur, M., Clement, B., et al., Proceedings of the Ocean Drilling Program, Scientific Results, Volume 105: College Station, Texas, Ocean Drilling Program, p. 137–154.

Bown, P.R., 2005, Palaeogene calcareous nannofossils from the Kilwa and Lindi areas of coastal Tanzania (Tanzania Drilling Project Sites 1 to 10, 2003–4): Journal of Nannoplankton Research, v. 27, p. 21–95.

Bown, P.R., and Young, J.R., 1998, Techniques, *in* Bown, P.R., ed., Calcareous Nannofossil Biostratigraphy. British Micropaleontological Society Publications Series: New York, Springer Sciences+Business Media, p. 16–21.

Burgess, C.E., Pearson, P.N., Lear, C.H., Morgans, H.E.G., Handley, L., Pancost, R.D., and Schouten, S., 2008, Middle Eocene climate cyclicity in the southern Pacific: Implications for global ice volume: Geology, v. 36, p. 651–654, doi:10.1130/G24762A.1.

Clement, B., and Hailwood, E., 1991, Magnetostratigraphy of sediments from Sites 701 and 702, *in* Ciesielski, P.F., Kristoffersen, Y., et al., Proceedings of the Ocean Drilling Program, Scientific Results, Volume 114: College Station, Texas, Ocean Drilling Program, p. 359–366.

Cogné, J.P., 2003, PaleoMac: A Macintosh™ application for treating paleomagnetic data and making plate reconstructions: Geochemistry Geophysics Geosystems, v. 4, p. 1–8, doi:10.1029/2001GC000227.

Cooper, R.A., 2004, The New Zealand Geological Timescale: Institute of Geological and Nuclear Sciences Monograph 22, 284 p.

Cramer, B.S., Wright, J.D., Kent, D.V., and Aubry, M.-P., 2003, Orbital climate forcing of $\delta^{13}C$ excursions in the late Paleocene–early Eocene (chrons C24n-C25n): Paleoceanography, v. 18, no. 4, p. 1–21, doi:10.1029/2003PA000909.

Crampton, J., Laird, M., Nicol, A., Townsend, D., and Van Dissen, R., 2003, Palinspastic reconstructions of southeastern Marlborough, New Zealand, for mid-Cretaceous–Eocene times: New Zealand Journal of Geology and Geophysics, v. 46, p. 153–175, doi:10.1080/00288306.2003.9515002.

Dallanave, E., Agnini, C., Muttoni, G., and Rio, D., 2009, Magneto-biostratigraphy of the Cicogna section (Italy): Implications for the late Paleocene–early Eocene time scale: Earth and Planetary Science Letters, v. 285, p. 39–51, doi:10.1016/j.epsl.2009.05.033.

Dallanave, E., Tauxe, L., Muttoni, G., and Rio, D., 2010, Silicate weathering machine at work: Rock magnetic data from the late Paleocene–early Eocene Cicogna section, Italy: Geochemistry Geophysics Geosystems, v. 11, no. 7, Q07008, doi:10.1029/2010GC003142.

Dallanave, E., Agnini, C., Muttoni, G., and Rio, D., 2012, Paleocene magneto-biostratigraphy and climate-controlled rock magnetism from the Belluno Basin, Tethys Ocean, Italy: Palaeogeography, Palaeoclimatology, Palaeoecology, v. 337–338, p. 130–142, doi:10.1016/j.palaeo.2012.04.007.

Deng, C., Zhu, R., Jackson, M.J., Verosub, K.L., and Singer, M.J., 2001, Variability of the temperature-dependent susceptibility of the Holocene eolian deposits in the Chinese loess plateau: A pedogenesis indicator: Physics and Chemistry of the Earth. Part A: Solid Earth and Geodesy, v. 26, p. 873–878, doi:10.1016/S1464-1895(01)00135-1.

Dickens, G.R., and Backman, J., 2013, Core alignment and composite depth scale for the lower Paleogene through uppermost Cretaceous interval at Deep Sea Drilling Project Site 577: Newsletters on Stratigraphy, v. 46, p. 47–68, doi:10.1127/0078-0421/2013/0027.

Edgar, K.M., Wilson, P.A., Sexton, P.F., Gibbs, S.J., Roberts, A.P., and Norris, R.D., 2010, New biostratigraphic, magnetostratigraphic and isotopic insights into the middle Eocene climatic optimum in low latitudes: Palaeogeography, Palaeoclimatology, Palaeoecology, v. 297, p. 670–682, doi:10.1016/j.palaeo.2010.09.016.

Ehrmann, W., 2001, Variations in smectite content and crystallinity in sediments from CRP-3, Victoria Land Basin, Antarctica: Terra Antartica, v. 8, p. 533–542.

Ehrmann, W., Melles, M., Kuhn, G., and Grobe, H., 1992, Significance of clay mineral assemblages in the Antarctic Ocean: Marine Geology, v. 107, p. 249–273, doi:10.1016/0025-3227(92)90075-S.

Ehrmann, W., Setti, M., and Marinoni, L., 2005, Clay minerals in Cenozoic sediments off Cape Roberts (McMurdo Sound, Antarctica) reveal palaeoclimatic history: Palaeogeography, Palaeoclimatology, Palaeoecology, v. 229, p. 187–211, doi:10.1016/j.palaeo.2005.06.022.

Fagel, N., 2007, Clay minerals, deep circulation and climate, *in* Hillaire-Marcel, C., and De Vernal, A., eds., Proxies in Late Cenozoic Paleoceanography: Developments in Marine Geology, Volume 1: Amsterdam, Elsevier, p. 139–184.

Fergusson, L.J., 1985, The Mineralogy, Geochemistry and Origin of lower Tertiary Smectite-Mudstones, East Coast Deformed Belt, New Zealand [Master's thesis]: Christchurch, New Zealand, University of Canterbury, New Zealand, 196 p.

Field, B.D., Uruski, C.I., Beu, A.G., Browne, G.H., Crampton, J.S., Funnell, R.H., Killops, S.D., Laird, M., Mazengarb, C., Morgans, H.E.G., Rait, G.J., Smale, D., and Strong, C.P., 1997, Cretaceous–Cenozoic Geology and Petroleum Systems of the East Coast Region: Institute of Geological & Nuclear Sciences Monograph 19, 310 p.

Fioroni, C., Villa, G., Persico, D., Wise, S.W., and Pea, L., 2012, Revised Middle Eocene–Upper Oligocene calcareous nannofossil biozonation for the Southern Ocean: Revue de Micropaleontologie, v. 55, p. 53–70, doi:10.1016/j.revmic.2012.03.001.

Fisher, R., 1953, Dispersion on a sphere: Proceedings of the Royal Society of London, v. A217, p. 295–305, doi:10.1098/rspa.1953.0064.

Florindo, F., and Roberts, A.P., 2005, Eocene-Oligocene magnetobiochronology of ODP Sites 689 and 690, Maud Rise, Weddell Sea, Antarctica: Geological Society of America Bulletin, v. 117, p. 46–66, doi:10.1130/B25541.1.

Föllmi, K., 1995, 160 my record of marine sedimentary phosphorus burial: Coupling of climate and continental weathering under greenhouse and icehouse conditions: Geology, v. 23, p. 503–506, doi:10.1130/0091-7613(1995)023<0503:MYROMS>2.3.CO;2.

Fornaciari, E., Agnini, C., Catanzariti, R., Rio, D., Bolla, E.M., and Valvasoni, E., 2010, Mid-latitude calcareous nannofossil biostratigraphy, biochronology and evolution across the middle to late Eocene transition: Stratigraphy, v. 7, no. 4, p. 229–264.

Galbrun, B., 1992, Magnetostratigraphy of Upper Cretaceous and Lower Tertiary sediments, Sites 761 and 762, Exmouth Plateau: Northwest Australia, *in* von Rad, U., Haq, B.U., et al., Scientific Results of the Ocean Drilling Program, Volume 122: College Station, Texas, Ocean Drilling Program, p. 699–716.

Gradstein, F.M., Ogg, J.G., Schmitz, M.D., and Ogg, G.M., 2012, The Geologic Time Scale 2012: Amsterdam, The Netherlands, Elsevier, 1144 p.

Hancock, H.J.L., Chaproniere, G.C., Dickens, G.R., and Henderson, R.A., 2002, Early Palaeogene planktic foraminiferal and carbon isotope stratigraphy, Hole 762C, Exmouth Plateau, northwest Australian margin: Journal of Micropalaeontology, v. 21, p. 29–42, doi:10.1144/jm.21.1.29.

Hancock, H.J.L., Dickens, G.R., Strong, C.P., Hollis, C.J., and Field, B.D., 2003, Foraminiferal and carbon isotope stratigraphy through the Paleocene-Eocene transition at Dee Stream, Marlborough, New Zealand: New Zealand Journal of Geology and Geophysics, v. 46, p. 1–19, doi:10.1080/00288306.2003.9514992.

Held, I.M., and Soden, B.J., 2006, Robust responses of the hydrological cycle to global warming: Journal of Climate, v. 19, p. 5686–5699, doi:10.1175/JCLI3990.1.

Hirt, A.M., and Gehring, A.U., 1991, Thermal alteration of the magnetic mineralogy in ferruginous rocks: Journal of Geophysical Research, v. 96, p. 9947–9953, doi:10.1029/91JB00573.

Hirt, A.M., Banin, A., and Gehring, A.U., 1993, Thermal generation of ferromagnetic minerals from iron-enriched smectites: Geophysical Journal International, v. 115, p. 1161–1168, doi:10.1111/j.1365-246X.1993.tb01518.x.

Hollis, C.J., Dickens, G.R., Field, B.D., Jones, C.M., and Strong, C.P., 2005a, The Paleocene-Eocene transition at Mead Stream, New Zealand: A southern Pacific record of early Cenozoic global change: Palaeogeography, Palaeoclimatology, Palaeoecology, v. 215, p. 313–343, doi:10.1016/j.palaeo.2004.09.011.

Hollis, C.J., Field, B.D., Jones, C.M., Strong, C.P., Wilson, G.J., and Dickens, G., 2005b, Biostratigraphy and carbon isotope stratigraphy of uppermost Cretaceous–lower Cenozoic Muzzle Group in middle Clarence Valley, New Zealand: Journal of the Royal Society of New Zealand, v. 35, p. 345–383, doi:10.1080/03014223.2005.9517789.

Hollis, C.J., Handley, L., Crouch, E.M., Morgans, H.E.G., Baker, J.A., Creech, J., Collins, K.S., Gibbs, S.J., Huber, M., Schouten, S., Zachos, J.C., and Pancost, R.D., 2009, Tropical sea temperatures in the high-latitude South Pacific during the Eocene: Geology, v. 37, p. 99–102, doi:10.1130/G25200A.1.

Hollis, C.J., Beu, A.G., Crampton, J.S., Crundwell, M.P., Morgans, H.E.G., Raine, J.I., Jones, C.M., and Boyes, A.F., 2010, Calibration of the New Zealand Cretaceous–Cenozoic Timescale to GTS2004: GNS Sciences Report 2010/43, 20 p.

Hollis, C.J., Taylor, K.W.R., Handley, L., Pancost, R.D., Huber, M., Creech, J.B., Hines, B.R., Crouch, E.M., Morgans, H.E.G., Crampton, J.S., Gibbs, S., Pearson, P.N., and Zachos, J.C., 2012, Early Paleogene temperature history of the southwest Pacific Ocean: Reconciling proxies and models: Earth and Planetary Science Letters, v. 349–350, p. 53–66, doi:10.1016/j.epsl.2012.06.024.

Hornibrook, N. de B., Brazier, R.C., and Strong, C.P., 1989, Manual of New Zealand Permian to Pleistocene Foraminiferal Biostratigraphy: New Zealand Geological Survey Paleontological Record, v. 56, p. 1–576.

Jones, C.H., 2002, User-driven integrated software lives: "Paleomag" paleomagnetics analysis on the Macin-

tosh: Computers & Geosciences, v. 28, p. 1145–1151, doi:10.1016/S0098-3004(02)00032-8.

Jovane, L., Florindo, F., Coccioni, R., Dinares-Turell, J., Marsili, A., Monechi, S., Roberts, A.P., and Sprovieri, M., 2007, The middle Eocene climatic optimum event in the Contessa Highway section, Umbrian Apennines, Italy: Geological Society of America Bulletin, v. 119, p. 413–427, doi:10.1130/B25917.1.

Kennett, J.P., and Stott, L.D., 1991, Abrupt deep-sea warming, paleoceanographic changes and benthic extinctions at the end of the Paleocene: Nature, v. 353, p. 225–229, doi:10.1038/353225a0.

Kent, D.V., and Muttoni, G., 2013, Modulation of Late Cretaceous and Cenozoic climate by variable drawdown of atmospheric pCO_2 from weathering of basaltic provinces on continents drifting through the equatorial humid belt: Climate of the Past, v. 9, p. 525–546, doi: 10.5194/cp-9-525-2013.

Kent, D.V., and Tauxe, L., 2005, Corrected Late Triassic latitudes for continents adjacent to the North Atlantic: Science, v. 307, p. 240–244, doi:10.1126/science.1105826.

Kent, D.V., Olsen, P.E., and Witte, W.K., 1995, Late Triassic–earliest Jurassic geomagnetic polarity sequence and paleolatitudes from drill cores in the Newark rift basin, eastern North America: Journal of Geophysical Research, v. 100, p. 14,965–14,998, doi:10.1029/95JB01054.

King, P.R., Naish, T.R., Browne, G.H., Field, B.D., and Edbrooke, S.W., 1999, Cretaceous to recent sedimentary patterns in New Zealand: Institute of Geological and Nuclear Science Folio Series, v. 1, p. 1–35.

King, R.F., 1955, The remanent magnetism of artificially deposited sediments: Geophysical Journal International, v. 7, supplement, p. 115–134, doi:10.1111/j.1365-246X.1955.tb06558.x.

Kirschvink, J.L., 1980, The least-squares line and plane and the analysis of palaeomagnetic data: Geophysical Journal of the Royal Astronomical Society, v. 62, p. 699–718, doi:10.1111/j.1365-246X.1980.tb02601.x.

Kodama, K., Fukuoka, M., Aita, Y., Sakai, T., Hori, R.S., Takemura, A., Campbell, H.J., Hollis, C.J., Grant-Mackie, J.A., and Spörli, K.B., 2007, Paleomagnetic results from Arrow Rocks in the framework of paleomagnetism in pre-Neogene rocks from New Zealand, *in* Spörli, K.B., Takemura, A., and Hori, R.S., eds., The Oceanic Permian/Triassic Boundary Sequence at Arrow Rocks (Oruatemanu), Northland, New Zealand: Lower Hutt, New Zealand, Geological and Nuclear Science Monograph 24, p. 177–196.

Krása, D., Petersen, K., and Petersen, N., 2007, Variable field translation balance, *in* Gubbins, D., and Herrero-Bervera, E., eds., Encyclopedia of Geomagnetism and Paleomagnetism: Dordrecht, The Netherlands, Springer, p. 977–979.

Kruiver, P., Dekkers, M., and Heslop, D., 2001, Quantification of magnetic coercivity components by the analysis of acquisition curves of isothermal remanent magnetization: Earth and Planetary Science Letters, v. 189, p. 269–276, doi:10.1016/S0012-821X(01)00367-3.

Kump, L.R., Brantley, S.L., and Arthur, M.A., 2000, Chemical weathering, atmospheric CO_2, and climate: Annual Review of Earth and Planetary Sciences, v. 28, p. 611–667, doi:10.1146/annurev.earth.28.1.611.

Little, T., and Roberts, A.P., 1997, Distribution and mechanism of Neogene to present-day vertical axis rotations, Pacific-Australian plate boundary zone, South Island, New Zealand: Journal of Geophysical Research, v. 102, p. 20,447–20,468, doi:10.1029/97JB01279.

Liu, Q., Deng, C., Yu, Y., Torrent, J., Jackson, M.J., Banerjee, S.K., and Zhu, R., 2005, Temperature dependence of magnetic susceptibility in an argon environment: Implications for pedogenesis of Chinese loess/palaeosols: Geophysical Journal International, v. 161, p. 102–112, doi:10.1111/j.1365-246X.2005.02564.x.

Lowrie, W., 1990, Identification of ferromagnetic minerals in a rock by coercivity and unblocking temperature properties: Geophysical Research Letters, v. 17, p. 159–162, doi:10.1029/GL017i002p00159.

Lowrie, W., and Alvarez, W., 1977, Upper Cretaceous–Paleocene magnetic stratigraphy at Gubbio, Italy: III. Magnetic stratigraphy: Geological Society of America Bulletin, v. 88, p. 374–377, doi:10.1130/0016-7606(1977)88<374:UCMSAG>2.0.CO;2.

Lyle, M., Wilson, P.A., and Janecek, T.R., 2002, Site 1220. Proceedings of the Ocean Drilling Program, Initial Reports, Volume 199: College Station, Texas, Ocean Drilling Program, p. 1–93.

Martini, E., 1971, Standard Tertiary and Quaternary calcareous nannoplankton zonation, *in* Farinacci, A., ed., Proceedings of the 2nd International Conference Planktonic Microfossils: Rome, Edizioni Tecnoscienza, p. 739–785.

McFadden, P.L., and McElhinny, M.W., 1990, Classification of the reversal test in palaeomagnetism: Geophysical Journal International, v. 103, p. 725–729, doi:10.1111/j.1365-246X.1990.tb05683.x.

McInerney, F.A., and Wing, S.L., 2011, The Paleocene-Eocene thermal maximum: A perturbation of carbon cycle, climate, and biosphere with implications for the future: Annual Review of Earth and Planetary Sciences, v. 39, p. 489–516, doi:10.1146/annurev-earth-040610-133431.

Meehl, G.A., Covey, C., Taylor, K.E., Delworth, T., Stouffer, R.J., Latif, M., McAvaney, B., and Mitchell, J.F.B., 2007a, The WCRP CMIP3 multimodel dataset: A new era in climate change research: Bulletin of the American Meteorological Society, v. 88, p. 1383–1394, doi: 10.1175/BAMS-88-9-1383.

Meehl, G.A., Stocker, T.F., Collins, W.D., Frielingstein, P., Gaye, A.T., Gregory, J.M., Kitoh, A., Knutti, R., Murphy, J.M., Noda, A., Raper, S.C.B., Watterson, I.G., Weaver, A.J., and Zhao, Z.-C., 2007b, Global climate projections, *in* Solomon, S., Qin, D., Manning, M., Chen, Z., Marquis, M., Averyt, K.B., and Tignor, M., eds., Climate Change 2007: The Physical Science Basis: Contribution of Working Group I to the Fourth Assessment Report of the Intergovernmental Panel on Climate Change: Cambridge, UK, Cambridge University Press, p. 747–846.

Morris, J.C., 1987, The Stratigraphy of the Amuri Limestone Group, East Marlborough, New Zealand [Ph.D. thesis]: Christchurch, New Zealand, University of Canterbury, New Zealand, 439 p.

Murphy, J.M., Sexton, D.M.H., Barnett, D.N., Jones, G.S., Webb, M.J., Collins, M., and Stainforth, D.A., 2004, Quantification of modelling uncertainties in a large ensemble of climate change simulations: Nature, v. 430, p. 768–772, doi:10.1038/nature02771.

Muttoni, G., Dallanave, E., and Channell, J.E.T., 2013, The drift history of Adria and Africa from 280 Ma to present, Jurassic true polar wander, and zonal climate control on Tethyan sedimentary facies: Palaeogeography, Palaeoclimatology, Palaeoecology, v. 386, p. 415–435, doi:10.1016/j.palaeo.2013.06.011.

Nicolo, M.J., Dickens, G.R., Hollis, C.J., and Zachos, J.C., 2007, Multiple early Eocene hyperthermals: Their sedimentary expression on the New Zealand continental margin and in the deep sea: Geology, v. 35, p. 699–702, doi:10.1130/G23648A.1.

Nicolo, M.J., Dickens, G.R., and Hollis, C.J., 2010, South Pacific intermediate water oxygen depletion at the onset of the Paleocene-Eocene thermal maximum as depicted in New Zealand margin sections: Paleoceanography, v. 25, p. 1–12, doi:10.1029/2009PA001904.

Ogg, J., and Bardot, L., 2001, Aptian through Eocene magnetostratigraphic correlation of the Blake Nose transect (Leg 171B), Florida continental margin, *in* Kroon, D., Norris, R.D., Klaus, A., et al., Proceedings of the Ocean Drilling Program, Scientific Results, Volume 171B: College Station, Texas, Ocean Drilling Program, p. 1–58.

Ogg, J., and Smith, A., 2012, The geomagnetic polarity time scale, *in* Gradstein, F.M., Ogg, J.G., Schmitz, M.D., and Ogg, G.M., eds., The Geologic Time Scale 2012: Amsterdam, The Netherlands, Elsevier, p. 85–113.

Okada, H., and Bukry, D., 1980, Supplementary modification and introduction of code numbers to the low-latitude coccolith biostratigraphic zonation (Bukry, 1973, 1975): Marine Micropaleontology, v. 5, p. 321–325, doi:10.1016/0377-8398(80)90016-X.

Pan, Y., Petersen, N., Winklhofer, M., Davila, A.F., Liu, Q., Frederichs, T., Hanzlik, M., and Zhu, R., 2005, Rock magnetic properties of uncultured magnetotactic bacteria: Earth and Planetary Science Letters, v. 237, p. 311–325, doi:10.1016/j.epsl.2005.06.029.

Pancost, R.D., Taylor, K.W.R., Inglis, G.N., Kennedy, E.M., Handley, L., Hollis, C.J., Crouch, E.M., Pross, J., Huber, M., Schouten, S., Pearson, P.N., Morgans, H.E.G., and Raine, J.I., 2013, Early Paleogene evolution of terrestrial climate in the SW Pacific, southern New Zealand: Geochemistry Geophysics Geosystems, v. 14, p. 1–17, doi:10.1002/2013GC004935.

Parès, J.M., and Lanci, L., 2004, A middle Eocene–early Miocene magnetic polarity stratigraphy in equatorial Pacific sediments (ODP Site 1220), *in* Channell, J.E.T., Kent, D.V., Lowrie, W., and Meert, J.G., eds., Timescales of the Paleomagnetic Field: American Geophysical Union Geophysical Monograph 145, p. 131–140.

Passier, H.F., de Lange, G.J., and Dekkers, M.J., 2001, Magnetic properties and geochemistry of the active oxidation front and the youngest sapropel in the eastern Mediterranean Sea: Geophysical Journal International, v. 145, p. 604–614, doi:10.1046/j.0956-540x.2001.01394.x.

Pearson, P.N., Olsson, R.K., Huber, B.T., Hemleben, C., and Berggren, W.A., 2006, Atlas of Eocene planktonic foraminifera: Lawrence, Kansas, Cushman Foundation for Foraminiferal Research Special Publication 41, 513 p.

Perch-Nielsen, K., 1985, Cenozoic calcareous nannofossils, *in* Bolli, H.M., Saunders, J.B., and Perch-Nielsen, K., eds., Plankton Stratigraphy: Cambridge, UK, Cambridge University Press, p. 427–554.

Peterson, B.J., Holmes, R.M., McClelland, J.W., Vörösmarty, C.J., Lammers, R.B., Shiklomanov, A.I., Shiklomanov, I.A., and Rahmstorf, S., 2002, Increasing river discharge to the Arctic Ocean: Science, v. 298, p. 2171–2173, doi:10.1126/science.1077445.

Potter, D., and Stephenson, A., 1986, The detection of fine particles of magnetite using anhysteretic and rotational remanent magnetizations: Geophysical Journal of the Royal Astronomical Society, v. 87, p. 569–582, doi:10.1111/j.1365-246X.1986.tb06638.x.

Pross, J., and 17 others, 2012, Persistent near-tropical warmth on the Antarctic continent during the early Eocene Epoch: Nature, v. 488, p. 73–77, doi:10.1038/nature11300.

Randall, K., Lamb, S., and Mac Niocaill, C., 2011, Large tectonic rotations in a wide zone of Neogene distributed dextral shear, northeastern South Island, New Zealand: Tectonophysics, v. 509, p. 165–180, doi:10.1016/j.tecto.2011.05.006.

Reay, M.B., 1993, Geology of the Middle Part of the Clarence Valley: Institute of Geological & Nuclear Sciences Geological Map 10, 144 p.

Roberts, A.P., Chang, L., Rowan, C.J., Horng, C.S., and Florindo, F., 2011, Magnetic properties of sedimentary greigite (Fe_3S_4): An update: Reviews of Geophysics, v. 49, RG1002, doi:10.1029/2010RG000336.

Roberts, A.P., Florindo, F., Chang, L., Heslop, D., Jovane, L., and Larrasoaña, J.C., 2013a, Magnetic properties of pelagic marine carbonates: Earth-Science Reviews, v. 127, p. 111–139, doi:10.1016/j.earscirev.2013.09.009.

Roberts, A.P., Sagnotti, L., Florindo, F., Bohaty, S.M., Verosub, K.L., Wilson, G.S., and Zachos, J.C., 2013b, Environmental magnetic record of paleoclimate, unroofing of the Transantarctic Mountains, and volcanism in late Eocene to early Miocene glaci-marine sediments from the Victoria Land Basin, Ross Sea, Antarctica: Journal of Geophysical Research–Solid Earth, v. 118, p. 1845–1861, doi:10.1002/jgrb.50151.

Sagnotti, L., Florindo, F., Verosub, K.L., Wilson, G.S., and Roberts, A.P., 1998, Environmental magnetic record of Antarctic palaeoclimate from Eocene/Oligocene glaciomarine sediments, Victoria Land Basin: Geophysical Journal International, v. 134, p. 653–662, doi: 10.1046/j.1365-246x.1998.00559.x.

Shackleton, N., Hall, M., and Bleil, U., 1985, Carbon-isotope stratigraphy, Site 577, *in* Turner, K.L., ed., Initial Reports of the Deep Sea Drilling Project, Volume 86: Washington, D.C., U.S. Government Printing Office, p. 503–511.

Shibuya, H., Merrill, D.L., and Hsu, V., 1991, Paleogene counterclockwise rotation of the Celebes Sea—Orien-

tation of ODP cores utilizing the secondary magnetization, *in* Silver, E.A., Rangin, C., von Breymann, M.T., et al., Proceedings of the Ocean Drilling Program, Scientific Results, Volume 124: College Station, Texas, Ocean Drilling Program, p. 519–523.

Slotnick, B.S., Dickens, G.R., Nicolo, M.J., Hollis, C.J., Crampton, J.S., Zachos, J.C., and Sluijs, A., 2012, Large-amplitude variations in carbon cycling and terrestrial weathering during the latest Paleocene and earliest Eocene: The record at Mead Stream, New Zealand: The Journal of Geology, v. 120, p. 487–505, doi:10.1086/666743.

Stephenson, A., 1980, Gyromagnetism and the remanence acquired by a rotating rock in an alternating field: Nature, v. 284, p. 48–49, doi:10.1038/284048a0.

Strong, C.P., Hollis, C.J., and Wilson, G.J., 1995, Foraminiferal, radiolarian, and dinoflagellate biostratigraphy of Late Cretaceous to middle Eocene pelagic sediments (Muzzle Group), Mead Stream, Marlborough, New Zealand: New Zealand Journal of Geology and Geophysics, v. 38, p. 171–209, doi:10.1080/00288306.1995.9514649.

Suganuma, Y., and Ogg, J., 2006, Campanian through Eocene magnetostratigraphy of Sites 1257–1261, ODP Leg 207, Demerara Rise (western Equatorial Atlantic), *in* Mosher, D.C., Erbacher, J., Malone, M.J., et al., Proceeding of the Ocean Drilling Program, Scientific Results, Volume 207: College Station, Texas, Ocean Drilling Program, p. 1–48.

Tan, X., Kodama, K.P., and Fang, D., 2002, Laboratory depositional and compaction-caused inclination errors carried by haematite and their implications in identifying inclination error of natural remanence in red beds: Geophysical Journal International, v. 151, p. 475–486, doi:10.1046/j.1365-246X.2002.01794.x.

Tauxe, L., 2005, Inclination flattening and the geocentric axial dipole hypothesis: Earth and Planetary Science Letters, v. 233, p. 247–261, doi:10.1016/j.epsl.2005.01.027.

Tauxe, L., 2010, Essentials of Paleomagnetism: Berkeley, California, University of California Press, 512 p.

Tauxe, L., and Kent, D.V., 1984, Properties of a detrital remanence carried by haematite from study of modern river deposits and laboratory redeposition experiments: Geophysical Journal of the Royal Astronomical Society, v. 76, p. 543–561, doi:10.1111/j.1365-246X.1984.tb01909.x.

Tauxe, L., and Kent, D.V., 2004, A simplified statistical model for the geomagnetic field and the detection of shallow bias in paleomagnetic inclinations: Was the ancient magnetic field dipolar?, *in* Channell, J.E.T., Kent, D.V., Lowrie, W., and Meert, J.G., eds., Timescales of the Paleomagnetic Field: American Geophysical Union Geophysical Monograph 145, p. 101–115.

Tauxe, L., and 30 others, 2012, Chronostratigraphic framework for the IODP Expedition 318 cores from the Wilkes Land margin: Constraints for paleoceanographic reconstruction: Paleoceanography, v. 27, PA2214, doi:10.1029/2012PA002308.

Thiry, M., 2000, Palaeoclimatic interpretation of clay minerals in marine deposits: An outlook from the continental origin: Earth-Science Reviews, v. 49, p. 201–221, doi:10.1016/S0012-8252(99)00054-9.

Thiry, M., and Jacquin, T., 1993, Clay mineral distribution related to rift activity, sea-level changes and paleoceanography in the Cretaceous of the Atlantic Ocean: Clay Minerals, v. 28, p. 61–84, doi:10.1180/claymin.1993.028.1.07.

Thomas, E., Barrera, E., Hamilton, N., Huber, B.T., Kennett, J.P., O'Connell, S.B., Pospichal, J.J., Spiess, V., Stott, L.D., Wei, W., and Wise, S.W., 1990, Upper Cretaceous–Paleogene stratigraphy of Sites 689 and 690, Maud Rise (Antarctica), *in* Barker, P.F., Kennet, J.P., et al., Proceedings of the Ocean Drilling Program, Scientific Results, Volume 113: College Station, Texas, Ocean Drilling Program, p. 901–914.

Toffanin, F., Agnini, C., Fornaciari, E., Rio, D., Giusberti, L., Luciani, V., Spofforth, D.J.A., and Pälike, H., 2011, Changes in calcareous nannofossil assemblages during the Middle Eocene Climatic Optimum: clues from the central-western Tethys (Alano section, NE Italy): Marine Micropaleontology, v. 81, p. 22–31, doi:10.1016/j.marmicro.2011.07.002.

Toffanin, F., Agnini, C., Rio, D., Acton, G., and Westerhold, T., 2013, Middle Eocene to early Oligocene calcareous nannofossil biostratigraphy at IODP Site U1333 (equatorial Pacific): Micropaleontology, v. 59, p. 1–14.

Villasante-Marcos, V., Hollis, C.J., Dickens, G.R., and Nicolo, M.J., 2009, Rock magnetic properties across the Paleocene-Eocene thermal maximum in Marlborough, New Zealand: Geologica Acta, v. 7, p. 229–242, doi:10.1344/105.000000280.

Walker, J.C.G., Hays, P.B., and Kasting, J.F., 1981, A negative feedback mechanism for the long-term stabilization of Earth's surface temperature: Journal of Geophysical Research, v. 86, p. 9776–9782, doi:10.1029/JC086iC10p09776.

Watson, G., 1983, Large sample theory of the Langevin distribution: Journal of Statistical Planning and Inference, v. 8, p. 245–256, doi:10.1016/0378-3758(83)90043-5.

Zachos, J.C., Pagani, M., Sloan, L., Thomas, E., and Billups, K., 2001, Trends, rhythms, and aberrations in global climate 65 Ma to present: Science, v. 292, p. 686–693, doi:10.1126/science.1059412.

Zachos, J.C., Dickens, G.R., and Zeebe, R.E., 2008, An early Cenozoic perspective on greenhouse warming and carbon-cycle dynamics: Nature, v. 451, p. 279–283, doi:10.1038/nature06588.

Zachos, J.C., McCarren, H., Murphy, B., Röhl, U., and Westerhold, T., 2010, Tempo and scale of late Paleocene and early Eocene carbon isotope cycles: Implications for the origin of hyperthermals: Earth and Planetary Science Letters, v. 299, p. 242–249, doi:10.1016/j.epsl.2010.09.004.

Zijderveld, J.D.A., 1967, A.C. demagnetization of rocks: Analysis of results, *in* Collinson, D.W., Creer, K.M., and Runcorn, S.K., eds., Methods in Paleomagnetism: New York, Elsevier, p. 254–286.

Science Editor: A. Hope Jahren
Associate Editor: Massimo Mattei

Manuscript Received 5 June 2014
Revised Manuscript Received 9 September 2014
Manuscript Accepted 20 October 2014

Printed in the USA